การสังเคราะห์ตัวเร่งปฏิกิริยาฐานเมโซพอรัสซิลิกาแบบสองและสามหน้าที่และการประยุกต์ในปฏิกิริยาต่อเนื่องเป็นขั้นแบบวันพอต

นายอภิชาติ คลายานนท์

วิทยานิพนธ์นี้เป็นส่วนหนึ่งของการศึกษาตามหลักสูตรปริญญาวิทยาศาสตรมหาบัณฑิต
สาขาวิชาเคมี ภาควิชาเคมี
คณะวิทยาศาสตร์ จุฬาลงกรณ์มหาวิทยาลัย
ปีการศึกษา 2560

SYNTHESIS OF BI- AND TRIFUNCTIONAL MESOPOROUS SILICA-BASED CATALYST AND APPLICATION IN ONE-POT CASCADE REACTIONS

Mr. Apichat Klayanon

A Thesis Submitted in Partial Fulfillment of the Requirements
for the Degree of Master of Science Program in Chemistry
Department of Chemistry
Faculty of Science
Chulalongkorn University
Academic Year 2017

Thesis Title	SYNTHESIS OF BI- AND TRIFUNCTIONAL MESOPOROUS SILICA-BASED CATALYST AND APPLICATION IN ONE-POT CASCADE REACTIONS
By	Mr. Apichat Klayanon
Field of Study	Chemistry
Thesis Advisor	Wipark Anutrasakda, Ph.D.

Accepted by the Faculty of Science, Chulalongkorn University in Partial Fulfillment of the Requirements for the Master's Degree

.....Dean of the Faculty of Science

(Professor Polkit Sangvanich, Ph.D.)

THESIS COMMITTEE

.....Chairman

(Associate Professor Vudhichai Parasuk, Ph.D.)

.....Thesis Advisor

(Wipark Anutrasakda, Ph.D.)

.....Examiner

(Duangamol Tungasmita, Ph.D.)

.....External Examiner

(Laksamee Chaicharoenwimolkul, Ph.D.)

อภิชาติ คลายานนท์ : การสังเคราะห์ตัวเร่งปฏิกิริยาฐานเมโซพอรัสซิลิกาแบบสองและสามหน้าที่และการประยุกต์ในปฏิกิริยาต่อเนื่องเป็นขั้นแบบวันพอต (SYNTHESIS OF BI- AND TRIFUNCTIONAL MESOPOROUS SILICA-BASED CATALYST AND APPLICATION IN ONE-POT CASCADE REACTIONS) อ. ที่ปรึกษาวิทยานิพนธ์หลัก: อ. ดร.วิภาค อนุตรศักดา, 85 หน้า.

งานวิจัยนี้รายงานการสังเคราะห์และการพิสูจน์เอกลักษณ์ของตัวเร่งปฏิกิริยาแบบสองหน้าที่ชนิดกรด-เบสของกรดซัลโฟนิคและเอมีนบนตัวรองรับเมโซพอรัสซิลิกาและตัวเร่งปฏิกิริยาแบบสามหน้าที่ชนิดกรด-เบส-โลหะบนตัวรองรับเมโซพอรัสซิลิการวมไปถึงการนำตัวเร่งปฏิกิริยาเหล่านี้ไปประยุกต์ใช้ กลุ่มของตัวเร่งปฏิกิริยาแบบสองหน้าที่ซึ่งถูกสังเคราะห์ให้แตกต่างกันในเรื่องตำแหน่งของกรด-เบส ปริมาณกรด-เบส และชนิดของอะมิโนไซเลนประกอบด้วย N_2SA_2, $SA_{0.5}N_{0.5}$, $SA_{0.5}N_2$, SA_1N_2, SA_2N_2, $SA_{0.5}N_4$, $SA_{0.5}NN_4$ และ $SA_{0.5}NNN_4$ โดยใช้วิธีโคคอนเดนเซชันร่วมกับวิธีกราฟติงในการสังเคราะห์ตัวเร่งปฏิกิริยาเหล่านี้ได้รับการพิสูจน์เอกลักษณ์ด้วยเทคนิคการเลี้ยวเบนของรังสีเอกซ์ เทคนิคอินฟราเรด เทคนิคการตรวจวัดพื้นที่ผิวและความมีรูพรุน กล้องจุลทรรศน์แบบส่องกราด กล้องจุลทรรศน์แบบส่องผ่าน เทคนิคการวิเคราะห์การเปลี่ยนแปลงน้ำหนักของสารโดยอาศัยคุณสมบัติทางความร้อนและสเปกโทรสโกปีของอนุภาคอิเล็กตรอนที่ถูกปลดปล่อยด้วยรังสีเอกซ์ ผลการวิเคราะห์พบว่าโครงสร้างหลักของวัสดุรองรับเมโซพอลัสซิลิกายังคงถูกรักษาไว้ภายหลังการดัดแปรพื้นผิวด้วยกรดและเบส โดยวัสดุที่สังเคราะห์ได้มีลักษณะภายนอกรูปร่างคล้ายถั่วแดงและมีความเป็นรูพรุนแบบเมโซชนิดหกเหลี่ยมค่อนข้างสูง ซึ่งมีพื้นที่ผิว ความเป็นกรด และความเป็นเบสอยู่ในช่วง 609 ถึง 729 ตารางเมตรต่อกรัม 0.88 ถึง 1.10 มิลลิโมลต่อกรัม และ 0.29 ถึง 0.57 มิลลิโมลต่อกรัม ตามลำดับ ตัวเร่งปฏิกิริยาเหล่านี้ถูกทดสอบโดยใช้ปฏิกิริยาดีอะซิทิลเลชันตามด้วยปฏิกิริยา Knoevenagel แบบต่อเนื่องในขั้นตอนเดียวที่อุณหภูมิ 90 องศาเซลเซียสเป็นเวลา 5 ชั่วโมง โดยใช้สารตั้งต้นเป็นเบนซัลดีไฮด์ไดเมทิลอะซิทัล (A) และมาโลโนไนไตรล์และสารผลิตภัณฑ์คือเบนซัลลิดีนมาโลโนไนไตรล์ (C) ผลจากการทดลองบ่งชี้ว่าการเปลี่ยนสารตั้งต้น A และการให้ผลผลิต C ได้รับอิทธิพลจากความเป็นกรด ความเป็นเบสและลักษณะเฉพาะของรูพรุนของตัวเร่งปฏิกิริยา ซึ่งตัวเร่งปฏิกิริยา $SA_{0.5}N_4$ แสดงประสิทธิภาพสูงที่สุดโดยให้ค่าการเปลี่ยนแปลงของ A ร้อยละ 100 และให้ผลิตภัณฑ์ C สูงถึงร้อยละ 71 นอกจากนี้ $SA_{0.5}N_4$ สามารถนำกลับมาใช้ซ้ำได้อย่างน้อย 4 ครั้งโดยไม่สูญเสียประสิทธิภาพในการเร่งปฏิกิริยาอย่างมีนัยสำคัญ

ตัวเร่งปฏิกิริยาแบบสองหน้าที่ที่มีประสิทธิภาพสูงสุดซึ่งคือ $SA_{0.5}N_4$ ถูกนำมาใช้ในการเตรียมวัสดุเมโซพอรัสซิลิกาแบบสามหน้าที่ชนิดกรด-เบส-โลหะ โดยใช้วิธีจุ่มชุ่มในการเติมโลหะแพลเลเดียมร้อยละ 0.03, 0.2 และ 1 โดยน้ำหนักลงไปบน $SA_{0.5}N_4$ จากนั้นตัวเร่งปฏิกิริยาแบบสามหน้าที่ถูกทดสอบประสิทธิภาพด้วยปฏิกิริยาดีอะซิทิลเลชัน Knoevenagel และไฮโดรจีเนชันแบบต่อเนื่องในขั้นตอนเดียวในการเปลี่ยน A ไปเป็นเบนซิลมาโลโนไนไตรล์ (D) โดยทำการศึกษาผลของเวลา ความดันแก๊สไฮโดรเจน ปริมาณโลหะแพลเลเดียมที่เติม และชนิดของอะมิโนไซเลน แต่อย่างไรก็ตามไม่พบสารผลิตภัณฑ์ D ด้วยการใช้ตัวเร่งปฏิกิริยาสามหน้าที่ภายใต้สภาวะใด ๆ แต่ผลิตภัณฑ์ D สามารถได้รับจากการใช้ตัวเร่งปฏิกิริยาผสมระหว่าง 5% ของโลหะแพลเลเดียมบนอลูมินาและ $SA_{0.5}N_4$ $SA_{0.5}NN_4$ หรือ $SA_{0.5}NNN_4$ โดยพบว่า ตัวเร่งปฏิกิริยาผสมระหว่าง $SA_{0.5}N_4$ และ5% ของโลหะแพลเลเดียมบนอลูมินาให้ประสิทธิภาพสูงที่สุดในการสังเคราะห์สาร D (ร้อยละ 49.4)

ภาควิชา เคมี ลายมือชื่อนิสิต .....

สาขาวิชา เคมี ลายมือชื่อ อ.ที่ปรึกษาหลัก .....

ปีการศึกษา 2560

5872090423 : MAJOR CHEMISTRY
KEYWORDS: MESOPOROUS SILICA / ACID-BASE CATALYST / BIFUNCTIONAL CATALYST / CASCADE REACTION / TRIFUNCTIONAL CATALYST / ACID-BASE-METAL CATALYST

APICHAT KLAYANON: SYNTHESIS OF BI- AND TRIFUNCTIONAL MESOPOROUS SILICA-BASED CATALYST AND APPLICATION IN ONE-POT CASCADE REACTIONS. ADVISOR: WIPARK ANUTRASAKDA, Ph.D., 85 pp.

This work reports the synthesis and full characterization of bifunctional mesoporous silica supported acid (-SO_3H)-base (-NH_2) catalysts and trifunctional mesoporous silica supported acid-base-metal catalysts as well as their applications. A series of bifunctional catalysts were synthesized with different site separations, acid loadings, base loadings and types of aminosilane, namely N_2SA_2, $SA_{0.5}N_{0.5}$, $SA_{0.5}N_2$, SA_1N_2, SA_2N_2, $SA_{0.5}N_4$, $SA_{0.5}NN_4$ and $SA_{0.5}NNN_4$, via a co-condensation and post-synthetic grafting methods and were characterized by XRD, FT-IR, N_2 adsorption-desorption, SEM, TEM, TGA and XPS techniques. The well-ordered hexagonal mesoporous structure was preserved throughout the synthesis where the synthesized materials exhibited small kidney-bean-shaped rod and highly ordered hexagonal mesoporous structures. The surface area, acidity, and basicity of the bifunctional catalysts were in the ranges of 609-729 $m^2 g^{-1}$, 0.88-1.10 mmol g^{-1}, and 0.29-0.57 mmole g^{-1}, respectively. These catalysts were tested in the one-pot deacetylation-Knoevenagel of benzaldehydedimethylacetal (A) with malononitrile to produce benzylidenemalononitrile (C) at 90 $^{\circ}C$ for 5 h. It was found that the conversion of A and the yield of C were influenced by the acidity, basicity and pore characteristics of the catalysts. In particular, The $SA_{0.5}N_4$ catalyst exhibited the highest conversion of A (100%) and the highest yield of C (71%) with good reusability of at least four cycles where no significant loss in catalytic activity was observed.

The best performing bifunctional catalyst was further used for the preparation of trifunctional catalysts, where the latter were prepared by impregnation of palladium metal (0.03, 0.2 and 1 wt.%) on the $SA_{0.5}N_4$ acid-base material. The trifunctional catalysts were tested in the one-pot deacetylation-Knoevenagel-hydrogenation of A to produce benzylmalononitrile (D). The effects of reaction time, hydrogen pressure, Pd loading and type of aminosilanes on the catalytic performance were investigated. Nevertheless, the desired product (D) was not observed in any treatment conditions. The production of D was, on the other hand, achieved by using the physical mixture of 5%Pd/Al_2O_3 and either of the $SA_{0.5}N_4$, $SA_{0.5}NN_4$, and $SA_{0.5}NNN_4$ catalysts. The $SA_{0.5}N_4$ catalyst continued to perform well for the one-pot production of D, where the highest yield of D (49.4 %) was achieved over the consecutive deacetylation-Knoevenagel-hydrogenation process catalyzed by the physical mixture of $SA_{0.5}N_4$ and 5%Pd/Al_2O_3.

Department: Chemistry
Field of Study: Chemistry
Academic Year: 2017

Student's Signature .....
Advisor's Signature .....

ACKNOWLEDGEMENTS

First of all, I would like to express my deepest gratitude to Dr. Wipark Anutrasakda, my advisor for his excellent guidance and invaluable advice in this research project. I am really thankful for his teaching and encouragement throughout the course of research.

I would like to gratefully thank the chairperson, Assoc. Prof. Dr. Vudhichai Parasuk and the thesis committee, Dr. Duangamol Tungasmita and Dr. Laksamee Chaicharoenwimolkul for all of their kindness and useful advice in the research.

I would like to thank the members of Materials Chemistry and Catalysis Research Unit for their willing helps and friendships, especially Ms. Kullatida Ratchadapiban, Ms. Padtaraporn Chanhom, Mr. Chawalit Takoon, Ms. Jamornpan Yangcharoenyuenyong and Ms. Apakorn Phasuk. Furthermore, I would like to give special thanks to Dr. Kunnigar Vongnam for her help, support and encouragement.

Finally, I would like to express my deepest gratitude to my family for their entirely care, understanding and financial support.

CONTENTS

Page

Page

Page

Page

Page

LIST OF TABLES

LIST OF FIGURES

LIST OF SCHEMES

LIST OF ABBREVIATIONS

SA	=	Sulfonic acid
N	=	3-aminopropyltriethoxysilane (APTES)
NN	=	[3-(2-aminoethylamino)propyltrimethoxysilane] (AAPTMS)
NNN	=	(Trimethoxysilylpropyl)diethylenetriamine (DETTMS)
MCM-41	=	Mobil Composition of Matter No. 41
μm	=	Micrometer
nm	=	Nanometer
wt.%	=	Percent by weight
mg	=	Milligram
g	=	Gram
mmole	=	Millimole
mL	=	Milliliter
μL	=	Microliter
L	=	Liter
M	=	Molar
°C	=	Degree Celsius
atm	=	Atmosphere
mm	=	Millimeter

LIST OF ABBREVIATIONS (Continued)

μm^2	=	Micro square meter
m^2	=	Square meter
cm^3	=	Cubic centimeter
E_a	=	Activation energy
Hz	=	Hertz
e.g.	=	Exempli gratia
D	=	Deuterated H

CHAPTER I

INTRODUCTION

1.1 Theory

1.1.1 Catalysts

A catalyst is a substance that can increase the rate of a reaction [1]. In general, a catalyst can lower the activation energy (E_a) of the reaction. Fig. 1.1 shows example profiles of a reaction with and without the addition of a catalyst. A single step was observed for the uncatalyzed reaction while a 4-step pathway was observed for the catalyzed reaction. It is clearly seen that the activation energy of the catalyzed reaction is lowered because each of the four steps has a lower-energy transition state than that of the uncatalyzed reaction [2].

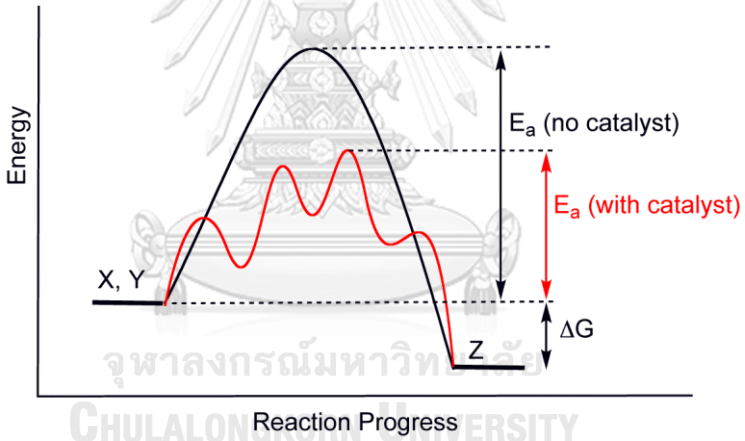

Figure 1.1 Profiles of a reaction with and without the addition of a catalyst [2].

The Maxwell-Boltzmann distribution is shown in Fig. 1.2. It is a plot between kinetic energy and the number of particles. Normally, the product of a reaction is formed when the energies of particles are equal to/higher than the activation energy (E_a). According to the diagram, the catalyst addition causes the lower activation energy and therefore the number of particles having higher energy than activation energy increases [3]. Consequently, the reaction rate is faster as a larger number of particles undergo successful collisions [4].

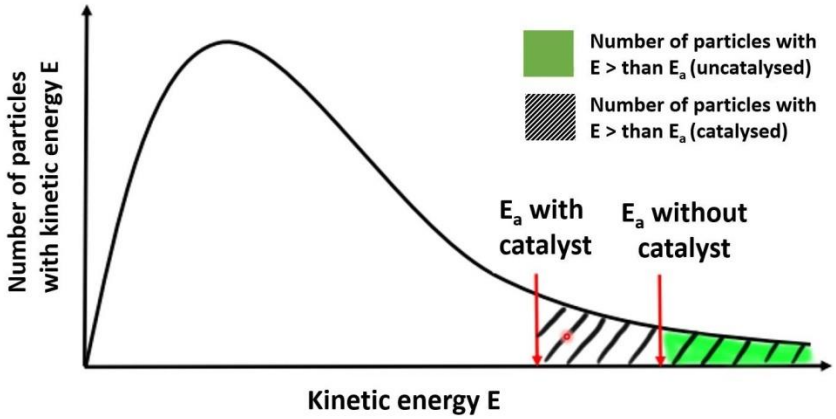

Figure 1.2 Maxwell-Boltzmann distribution curve [5].

1.1.1.1 Type of catalysts

Generally, there are two types of catalysts: homogeneous catalysts and heterogeneous catalysts.

1.1.1.1.1 Homogeneous catalysts

A homogeneous catalyst and reactants are in the same phase. Typically, homogeneous catalysts are present as a gas or liquid phase [6]. The advantage of homogeneous catalysts is high selectivity compared to heterogeneous catalysts. However, the separation of the catalyst is more difficult at the end of the process. In other words, it is difficult to recover the catalyst [7].

1.1.1.1.2 Heterogeneous catalysts

A heterogeneous catalyst and reactants are in a different phase. In general, heterogeneous catalysts are in a solid phase whereas reactants are in a liquid or gas phase [8]. Porous materials are commonly used as supporting materials in heterogeneous catalysts [9, 10]. The activity of heterogeneous catalysts can be occurred on the surface of materials and then the reactants are absorbed as shown in the Fig. 1.3. The mechanism of the heterogeneous catalysis includes five steps [11]:

(1) The reactants are diffused to the catalyst surface.

(2) The reactants are adsorbed on the catalyst surface.

(3) The reaction occurs on the surface of catalyst to generate products.

(4) The products generated on the surface of catalyst are desorbed.

(5) The products are diffused into the surrounding medium.

Normally, homogeneous catalysts have higher catalytic activity than heterogeneous catalysts because when the starting materials occupy onto the surface of catalyst, the reaction cannot proceed until products leave the surface, and new reactant molecules can adsorb on space available again, but the major advantages of heterogeneous catalysts are high stability at high temperature and ease to remove from the reactants and products by filtration [12, 13]. For these reasons, the adsorption step in a heterogeneously catalyzed reaction is the rate-limiting step [14]. Table 1.1 shows the properties of homogeneous and heterogeneous catalysts.

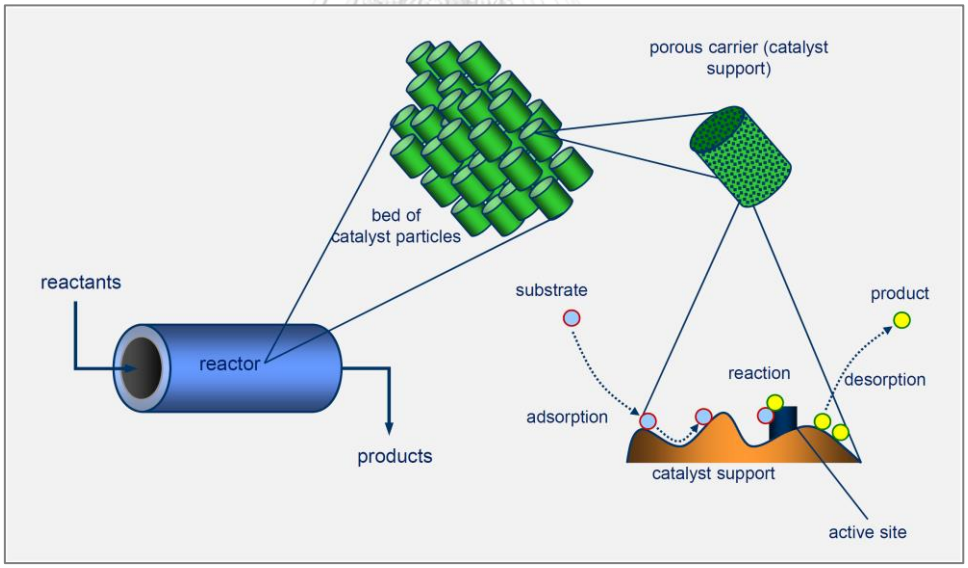

Figure 1.3 The mechanism of the heterogeneous catalysis reactions [15].

Table 1.1 The differences between homogeneous and heterogeneous catalysts [16]

Factors	Homogenous catalyst	Heterogeneous catalyst
Actives sites	All atom (no phase boundaries)	Only active surface atom
Phase	Liquid	Gas/solid
Temperature	Low (<250 ^{0}C)	High (250-500 ^{0}C)
Selectivity	High	Low
Diffusion	Facile	Can be very important
Heat transfer	Facile	Can be problematic
Reusability	A lack of reusability	Easy to be reused by filtration/centrifugation
Catalyst modification	Easy	Difficult
Reaction mechanisms	Reasonably well understood	Poorly understood

1.1.2 Porous materials

Porous materials can be used as drug delivery, adsorbents, sensors, and catalyst supports because they have high surface areas [17]. There are three types of porous materials (Table 1.2) according to International Union of Pure Applied Chemistry (IUPAC).

Table 1.2 IUPAC classification of porous materials [18]

Type of porous material	Pore diameter
Micropore	< 2 nm
Mesopore	2 – 50 nm
Macropore	> 50 nm

The pore sizes of zeolites are normally in the range of 0.2-1.0 nm, considered as microporous materials [19]. Their major limitation is poor diffusion due to small micropores. In order to solve this problem, mesoporous materials have been developed and used in many reactions.

1.1.3 Mesoporous materials

Pore diameters of mesoporous materials are in the range of 2 to 50 nm. Examples of mesoporous materials are hexagonal MCM-41, cubic MCM-48 and lamellar MCM-50 (Fig. 1.4).

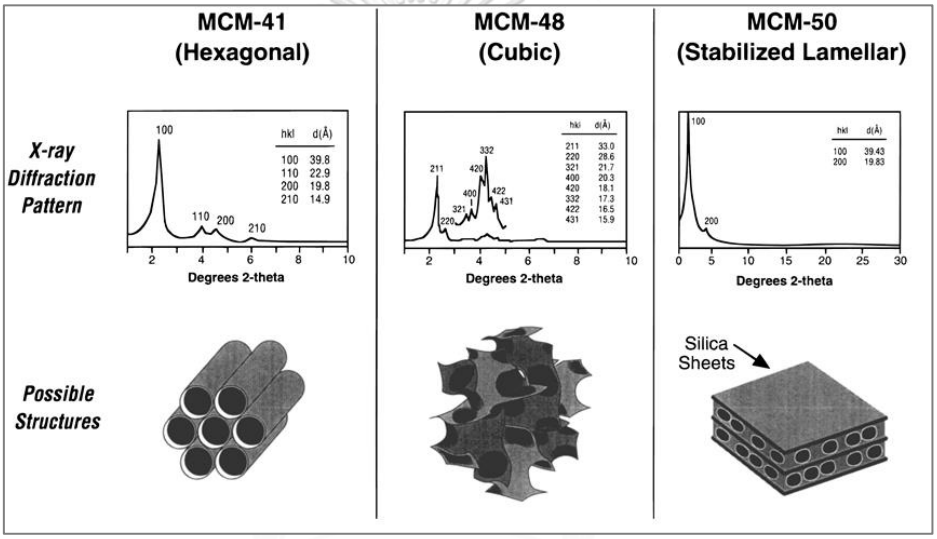

Figure 1.4 The X-ray diffraction patterns and structures of MCM-41, MCM-48 and MCM-50 [20].

1.1.3.1 Synthetic strategies of mesoporous materials

The creation of mesoporous materials is dependent on the interaction between organic species (surfactant or template) and inorganic species (silica source). Usually, the surfactants are amphiphilic molecules, meaning that they contain both hydrophilic head groups and hydrophobic tail groups [21] as shown in Fig. 1.5.

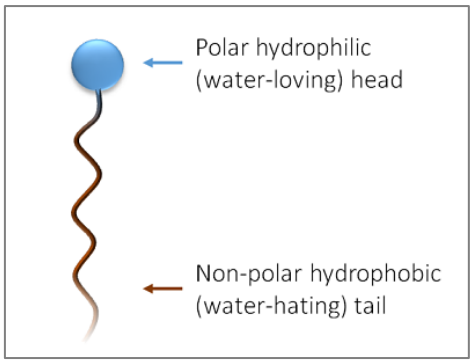

Figure 1.5 A surfactant molecule structure [22].

Surfactants can be classified into three categories according to the charges of the head groups [23]:

(I) Anionic surfactants (S^-) are composed of negatively charged head groups such as alkyl carboxylate, phosphate, sulfate and sulphonate.

(II) Cationic surfactants (S^+) are composed of positively charged head groups, including alkyl quaternary ammonium salt.

(III) Non-ionic surfactants (S^0) are composed of electrostatic neutral head groups, including ethyloxide/propyloxide diblock or triblock coployers, alkyl polyesters and alkyl amines.

The surfactant charging (S) is dependent on the charges of the head groups whereas the charging of silica species (I) is dependent on pH of the synthesis system (1.2). Silica species is neutral at its isoelectric point, under the conditions that pH < 1.2, silica species are positively charged (I^+), while when pH > 1.2, the silica species are negatively charged (I^-) [24]. As shown in Fig. 1.6, electrostatic forces are interaction between the head groups and inorganic species with charge (1.6a-1.6d) while 1.6e-1.6f are hydrogen bonding between that two species.

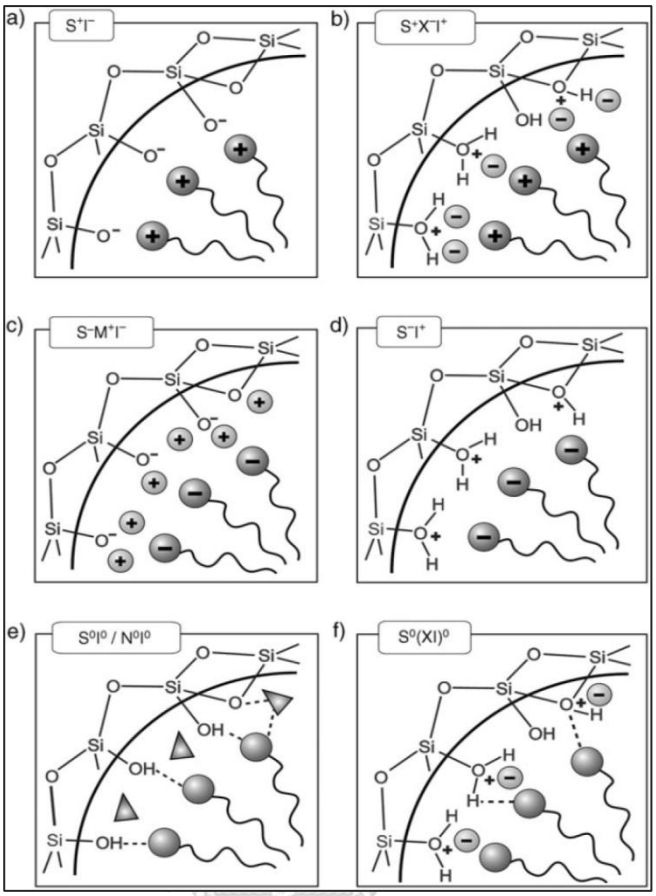

Figure 1.6 Interface interactions between the inorganic phase (I) and the organic phase (S, N): (**a**–**d**) ionic interactions; (**e**) and (**f**) hydrogen bonding [25]. (Dash line refereshydrogen bond).

1.1.3.2 Mechanistic formation of mesoporous materials

Normally, a quarternary ammonium surfactant is used as an ionic template for synthesizing hexagonal MCM-41 mesoporous materials. Pore size about 2 to 10 nm were made by using a template of cetyltrimethylammonium bromide (CTAB) [26, 27]. There are two pathways to generate mesoporous materials as shown in Fig 1.7. The first pathway is surfactant liquid crystals; micelles forming by introducing of template to create mesopores. Then, the hydrophilic part of the template is deposited by the inorganic species, followed by the elimination of template to obtain mesoporous silica materials. The second pathway is cooperative

self-assembly; surfactant of mesopores forming by adding the silica source, which controls the self-assembly process.

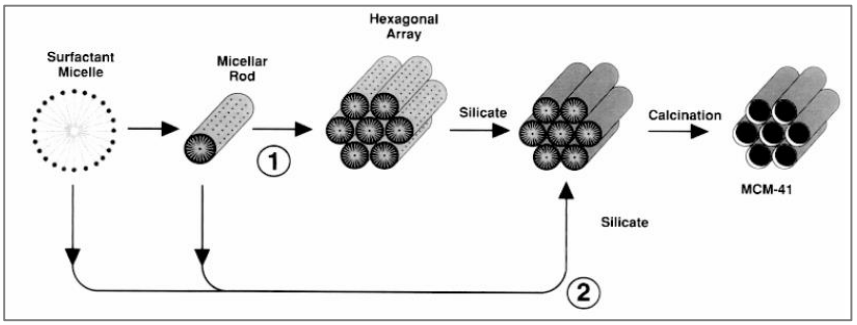

Figure 1.7 Two MCM-41 formation pathways: (1) liquid crystal phase and (2) cooperative self-assembly [26].

1.1.4 Functionalization of mesoporous silicas

The efficiency of mesoporous material was increased by functionalization with organic groups on their surface. There are two methods based on organosilica units for functionalization: grafting method and co-condensation method.

1.1.4.1 Grafting method

Grafting method is a post-synthesis method, which involves organosilanes, $(OR')_3SiR$, reacting with the free silanol groups at pore surfaces as shown in Fig. 1.8. The use of this method leads to the retained structure of the silica phase under the synthetic conditions. Whereas the organosilanes react mainly at the opening of the pores, the diffusion of additional molecules the pores was limited, resulting in a heterogeneous distribution of the organic moieties in the pores, and pore blockage [28].

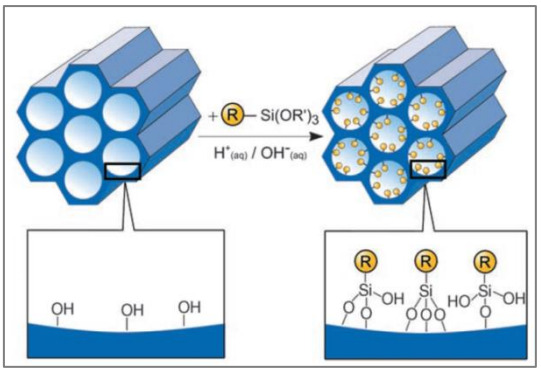

Figure 1.8 Grafting (post-synthetic functionalization) for mesoporous pure silica phases with $(R'O)_3SiR$ organosilanes [29].

1.1.4.2 Co-condensation method

Co-condensation is a one-pot synthesis method, which is used for preparing mesoporous structure from tetraalkoxysilanes ($(RO)_4Si$, TEOS) with terminal trialkoxyorganosilanes ($(R'O)_3SiR$) as shown in Fig. 1.9. Pore blocking cannot occur in this method because the organic functionalities are direct components of the silica matrix. Moreover, the textural properties of materials are decreased with increasing in loading of the organic groups. In addition, the extraction is the only method that can be used for elimination of the template because calcination is not suitable in this case due to the requirement of high temperature [30].

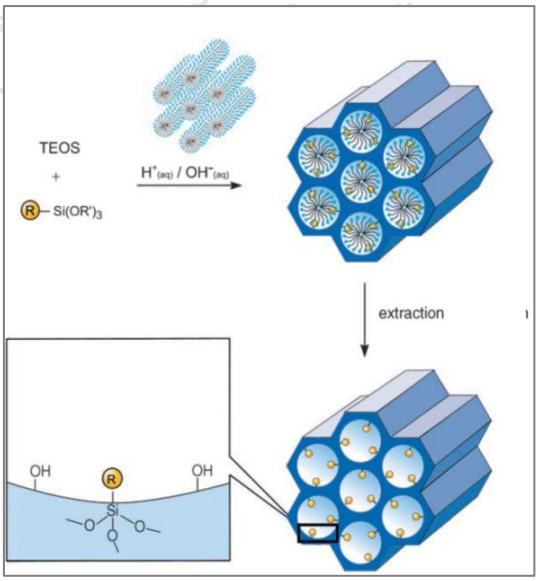

Figure 1.9 The organic modification of mesoporous pure silica phases by co-condensation [29].

1.1.5 Applications of functionalized mesoporous silicas for catalysis

High surface area and pore size of 2-50 nm of mesoporous materials are frequently used as supports for immobilizing catalytic species so that the overall catalytic performance in the catalytic processes is improved.

The advantages of using a functionalize mesoporous silica as catalyst include:

1) Solid catalyst and reactants are in in different phases; therefore, it is easier to separate the catalyst from the liquid process by filtration.

2) The catalyst can be regenerated and reused.

3) Limitation of size and shape of the catalyst within mesopores provides selectivity and specificity for a reaction.

Due to these advantages, catalytic systems based on mesoporous silica were used and applied in a lot of catalysis systems [31-33]. Suzuki et al. [34] synthesized amino-functionalized mesoporous silica with three types of organosilanes: aminopropyl (N), ethylene-diamine (NN), and diethylene-triamine (NNN) silanes. Catalytic activity of the synthesized materials was examined by nitroaldol condensation reaction of *p*-hydroxybenzaldehyde with nitromethane. The results showed that the material functionalized with aminopropyl (N) had the largest pore size, surface area, and pore volume. The order of catalytic activity is: 91% (N) > 83% (NN) > 60% (NNN). Interestingly, aminopropyl (N)-functionalized catalyst exhibited a higher reactivity than the other two catalysts because it contained the smallest aminosilane molecules, which were less steric hindrance in the reaction.

1.1.6 Multifunctional catalysts for cascade reactions

One of the interesting topics in chemistry is the development and improvement of the environmentally friendly technologies such as time saving, decreased waste, decreased solvent and low operation cost. This problem can be overcome by using recyclable feedstock of catalysts [35].

One of the most of natural catalysts is enzyme, which are often held as a benchmark of living systems in terms of performance [36]. The nature of

enzyme can catalyze several cascade reactions under mild and same conditions in one pot [37]. Although, they have high selectivity of multifunctional catalysts but the kinetics of the reaction is slow in large scale productions. The improvement in the terms of decreasing of energy consuming in each step is the economic application of a chemical manufacturing process. Consequently, the processes become green, attractive with a reduced waste production [38]. In this objective, heterogeneous catalysts are attractive catalysts to efficiently perform in multistep processes.

A major important in the multifunctional solid catalysts is stability of active sites from chemically interfering under the reaction processes. This would specify the reaction conditions to obtain the final products. All active sites required on a single catalyst or physical mixture to get different catalysts. In addition, the balance of each active site is important in multistep process.

In 2006, Alauzun and co-workers [39] synthesized bifunctional mesoporous material containing two different active sites: acidic groups in the framework and basic groups in pores by the co-condensation method. Then, disulfide was reduced, followed by oxidation to SO_3H groups, and deprotection of amino groups.

In addition, other examples of bifunctional catalysts are: dehydrohalogenation–hydrogenation reactions by sol–gel materials [40], isolated active sites on clay materials catalyzed acid–base series reactions [41], resin-supported acidic and basic catalysts used in a one-pot sequence deacetalization and enantioselective aldol reaction [42], palladium-supported catalyst on a magnetically separable composite and a cross-linked sulfonic acid polystyrene for a dehydration–hydrogenation tandem [43].

1.2 Literature reviews on bi- and trifunctional catalysts

1.2.1 Bifunctional catalysts with difference active sites

1.2.1.1 Bifunctional catalysts of acid-base sites

Zhang et al. [44] prepared amine-grafted graphene oxide (GOAP) containing phosphotungstic acid through silylanization and electrostatic

interaction for testing its catalytic activity between benzaldehyde dimethyl acetal and nitromethane to produce trans-β-nitrostyrene in a one-pot deacetalization–nitroaldol reaction (Scheme 1.1). The conversion and the yield of the final product were 100% and 99.2%, respectively under GOAP (acid/base weight ratio of 0.2:1) at at 100 °C for 18 h.

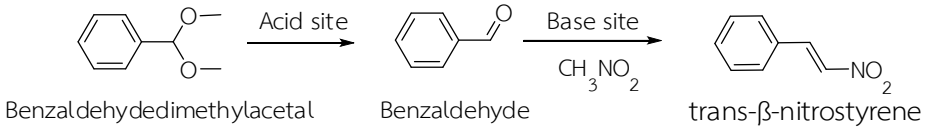

Scheme 1.1 One-pot of deacetalization–nitroaldol reaction.

Elmekawy et al. [45] compared two solid bifunctional catalysts (acid-base) for the one-pot deacetalization-nitroaldol reaction (Scheme 1.1). The first one was NH_2-SiO_2-SO_3H catalyst by grafting mercaptopropyl units and aminopropyl groups to the silica surface. The other one was NH_2-SiO_2-PTA by grafting only aminopropyl groups and then partially neutralizing with phosphotungstic acid. The NH_2-SiO_2-SO_3H catalyst showed higher activities than NH_2-SiO_2-PTA catalyst because sulfonic acid has an ability to donate protons to the obtained product from the deacetalization reaction. Consequently, this ability promotes the performance of the base site in nitroaldol reaction while phosphotungstic acid cannot.

1.2.1.2 Bifunctional catalysts of acid-metal sites

Iosif et al. [46] synthesized bifunctional catalysts of beta-zeolites impregnated with iridium (3% Ir/H-Beta zeolite) as catalyst in one-pot reaction of menthol from citronellal as shown in Scheme 1.2. There are two steps involved in this process, which are acid-catalyzed cyclization of citronellal to isopulegol and metal-catalyzed hydrogenation of the double bond in isopulegol to menthol. The first acid-cyclization step was performed under N_2 atmosphere for 4 h at 80 ℃ and the reactor was then added with H_2 atmosphere under 8 bar for 30 h. The conversion of citronellal and the selectivity of menthol were 100% and 95%, respectively.

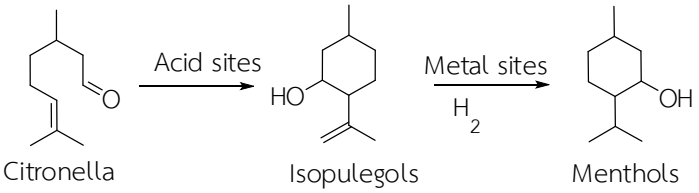

Scheme 1.2 One-pot of cyclization-hydrogenation reaction.

1.2.1.3 Bifunctional catalysts of base-metal sites

Li et al. [47] prepared Fe_3O_4-NH_2-Pd containing Pd nanoparticles, an amino group functionalized mesoporous silica nanosphere, and superparamagnetic Fe_3O_4 nanoparticles. The catalyst was tested in the one-pot Knoevenagel-hydrogenation reaction under H_2 bubbling (80 mL min^{-1}) for 1 h (Scheme 1.3). The cyclohexanone was converted to 2-cyclohexylmalononitrile with 100% conversion and ~100% yield. The catalyst was also separated by a simple magnetic separation.

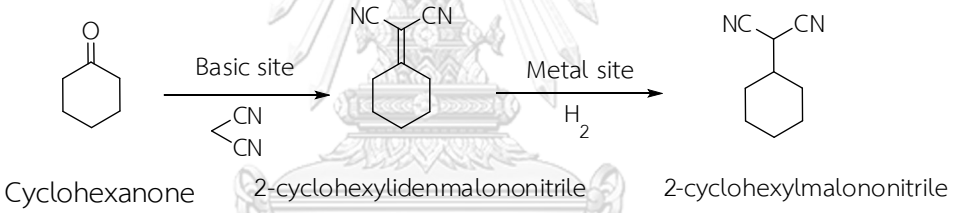

Scheme 1.3 One-pot of Knoevenagel-hydrogenation reaction.

Many bifunctional catalysts have demonstrated the outstanding improvement in catalytic activities with designed catalysts, which are able to transform a reactant of interest to a desired product in a one-pot two-step reaction. Based on these successful syntheses of bifunctional catalysts, it is interesting to further explore the possibility of the synthesis and utilization of trifunctional catalysts.

1.2.2 Trifunctional catalysts containing acid, base and metal

1.2.2.1 Physical mixture of acid, base and metal

The multiple combinations of catalysts for cascade reactions were reported. For example, Phan et al. [48] investigated the use of multiple catalysts in one-pot cascade reactions. The sulfonic acid polymer resin was

combined with basic catalyst of superparamagnetic spinel ferrite nanoparticles functionalized with amino groups and 0.5% Pt/Al_2O_3 included in a membrane in the three-step reaction sequence deacetalization-Knoevenagel-hydrogenation (Scheme 1.4). The reaction was tested under atmosphere for 1 h, then the H_2 pressure was increased to 69 bar at room temperature for 48 h. The result showed that the yield of benzylmalononitrile was 78%. After the end of reaction, the catalysts were easily separated from the reaction.

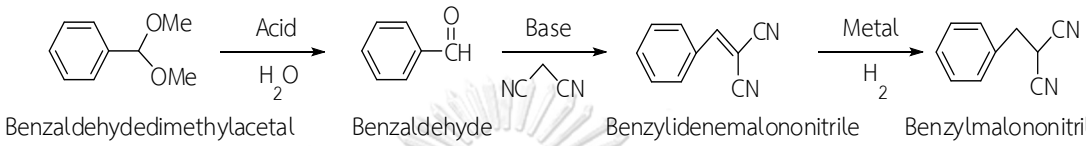

Scheme 1.4 One-pot of deacetalization-Knoevenagel–hydrogenation reaction.

1.2.2.2 Trifunctional catalysts in a single material

1.2.2.2.1 Trifunctional catalysts of base-acid-metal sites

Chen et al. [49] synthesized Mg/Al hydrotalcites (CHT) with various atomic ratios of Mg/Al supported palladium (Pd/CHT) or nickel (Ni/CHT) catalysts. Methyl isobutyl ketone (MIBK) was synthesized from acetone and hydrogen in the one-pot aldol condensation-dehydration-hydrogenation reaction (Scheme 1.5). The results showed that 35-40% of conversion and 60-70% of product selectivity were obtained. The optimum metal loading was 0.2 wt.% for Pd/CHT and 3 wt.% for Ni/CHT catalysts. However, the decreasing in catalytic activity of 0.2%Pd/CHT from 37% to 26% of conversion was because both catalysts had poor stability in gas-phase synthesis of MIBK.

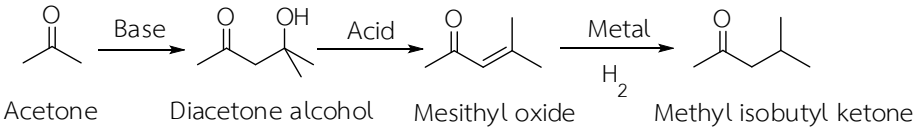

Scheme 1.5 One-pot of aldol condensation-dehydration-hydrogenation.

1.2.2.2.2 Trifunctional catalyst of acid-base-metal sites

Biradar et el. [50] reported the preparation of a trifunctional catalyst containing three catalytic groups: amine, sulphonic acid and Pd nanoparticle anchored on SBA-15 (named Pd-SO_3H-NH_2-SBA-15). The catalyst could convert benzaldehydedimethylacetal to 2-phenylethanamine in the one-pot process

via three consecutive reactions: deacetylation, Henry, and hydrogenation reactions (Scheme 1.6). The catalyst was tested in a flask with a balloon containing H_2 and it gave 100% conversion with 29% selectivity of final product. In addition, when 2 bar of H_2 pressure was used, a 100% of conversion and 92% of selectivity were obtained.

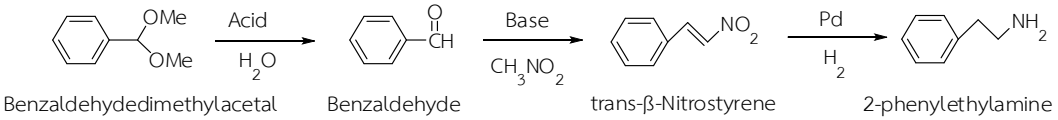

Scheme 1.6 One-pot of deacetalization-Henry condensation–hydrogenation reaction.

1.2.3 Synthesis of benzylmalononitrile

Scheme 1.7 One-pot of reductive alkylation.

Benzylmalononitrile is an important pharmaceutical intermediate, which can be used in the synthesis of antimalarial drugs [51]. As shown in Table 1.3, the price of benzylmalononitrile is high (17,800 bahts per gram). Therefore, it is interesting to develop a cost-effective synthetic method for the synthesis of benzylmalononitrile. As previously reported, benzylmalononitrile can be synthesized from benzaldehyde with malononitrile in a two-step one-pot process by reductive alkylation reaction (Scheme 1.7). It will increase the value of chemical about 712 times from 24 baht / gram to 17800 baht / gram.

Table 1.3 Price of chemicals (THB/g)

Chemicals	Prices (THB/g)
Benzaldehydedimethylacetal (**A**)	19
Benzaldehyde (**B**)	24
Benzylidenemalononitrile (**C**)	100
Benzylmalononitrile (**D**)	17800

A, B, C purchased from http://www.sigmaaldrich.com

D purchased form www.dskbiopharma.com

Sammelson et al. [52] synthesized benzylmalononitrile by reductive alkylation of malononitrile with benzaldehyde using sodium borohydride ($NaBH_4$) as reducing agent. The reactions was performed using water as the catalyst in ethanol for the condensation step, followed by the reduction step taking place effectively with $NaBH_4$ to produce benzylmalononitrile with the yield of 85% from the filtration method and of 98% from the extraction method. However, the condition under $NaBH_4$ had the disadvantages because of high cost. In addition, the residue of borate could cause the wastewater by nature.

Zhang et al. [53] used Hantzsch (1,4-dihydropyridine) as the reductant, in the direct reductive benzylizations of malononitrile for 90 min. The results showed that 68% yield of benzylmalononitrile was obtained with diethyl 2,6-dimethylpyridine-3,5-dicarboxylate as a by-product.

Wu et al. [54] reported the one-step reductive alkylation of benzaldehyde with malononitrile, which proceeded under $[Cp^*RhCl_2]_2$ catalysis transfer hydrogenation condition using $HCOOH–Et_3N$ as the hydrogen source. The results showed that benzylmalononitrile could be produced as the only product in 90% yield within 1 h at 40 $^{\circ}C$.

Jimenez et al. [55] synthesized benzylidenemalononitrile through Knoevenagel condensation by microwave radiation under the conditions of 20 W, 60 $^{\circ}C$ and 30 min using methanol as solvent. Then, Penicillium citrinum CBMAI 1186 was used in the reduction of the C=C bond. The mixtures were left for 6 days at 32 $^{\circ}C$. The final products were obtained in 97% yield of benzylmalononitrile.

According to the literature reviews described above, many researchers successfully developed methods for converting benzaldehyde (**B**) to benzylmalononitrile (**D**) in high yields. However, the synthetic processes of **D** were quite more complicated, difficult to separate the catalyst at the end of the process, and a lack of catalyst reusability. Therefore, the development of a method for the synthesis of **D** by using benzaldehydedimethylacetal (**A**) as the staring material in one-pot reaction and the capability of catalyst reusability are interesting and

challenging. Moreover, this process is also considered as a production of a value-added chemical as well (**A** 19 baht/g to **D** 17800 baht/g).

In this work, we prepared trifunctional acid-base-metal mesoporous catalysts (sulfonic acid-amine-palladium). Sulfonic acid was used as the acid sites, three aminosilanes with different numbers of amino groups were used as base sites. Then, palladium, as the metallic sites, was anchored on the obtained acid-base materials. Finally, the synthesized materials were tested as heterogeneous catalysts in the one-pot deacetalization-Knoevenagel-hydrogenation reaction of **A** with malononitrile to produce **D** as the final product (Scheme 1.8).

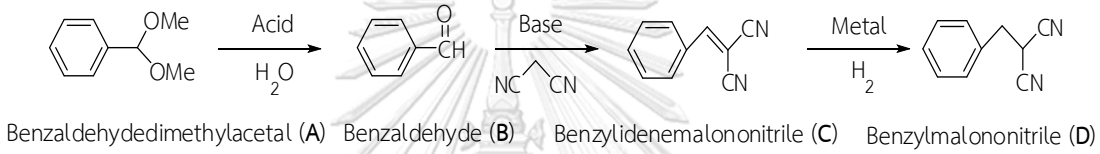

Benzaldehydedimethylacetal (**A**) Benzaldehyde (**B**) Benzylidenemalononitrile (**C**) Benzylmalononitrile (**D**)

Scheme 1.8 One-pot of deacetalization-Knoevenagel-hydrogenation.

1.3 Objectives

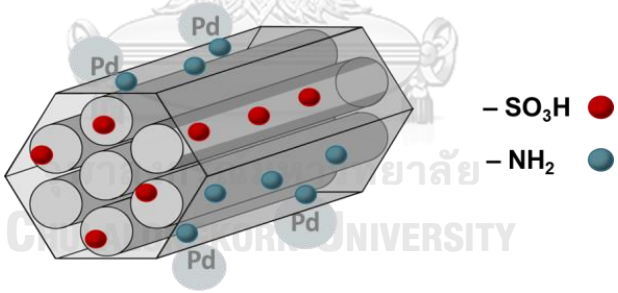

Figure 1.10 Trifunctional of acid-base-metal mesoporous catalysts.

1. To prepare and characterize a series of bifunctional mesoporous silica materials using sulfonic acid as the acid sites and three types of aminosilanes as the base sites.

2. To study the catalytic activities of the synthesized bifunctional materials as heterogeneous catalysts for their catalytic activities in the one-pot deacetalization-Knoevenagel reaction of benzaldehydedimethylacetal (**A**) with malononitrile to produce benzylidenemalononitrile (**C**).

3. To prepare and characterize a series of trifunctional mesoporous silica materials using sulfonic acid as the acid sites, three types of aminosilanes as the base sites and palladium as the metallic sites.

4. To examine the catalytic processes of the synthesized trifunctional materials as heterogeneous catalysts for their catalytic activities in one-pot deacetalization-Knoevenagel-hydrogenation reaction of benzaldehydedimethylacetal (**A**) with malononitrile to produce benzylmalononitrile (**D**).

1.4 Scope

This research reported on the synthesis and characterization of a series of bi- and trifunctional mesoporous silica materials using sulfonic acid as the acid sites, three types of aminosilanes: APTES (N), AAPTMS (NN), and DETTMS (NNN) as the base sites, and palladium as the metallic sites. Then, the synthesized bi- and trifunctional materials was tested and compared their catalytic activities in one-pot deacetylation and Knoevenagel reaction of benzaldehydedimethylacetal (**A**) with malononitrile to produce benzylidenemalononitrile (**C**) and the one-pot deacetalization-Knoevenagel-hydrogenation reaction of benzaldehydedimethylacetal (**A**) with malononitrile to produce benzylmalononitrile (**D**), respectively.

CHAPTER II

EXPERIMENTS

2.1 Apparatus and analytical techniques

2.1.1 Powder X-ray diffraction (XRD)

Rigaku, Dmax 2200/utima+ X-ray powder diffractometer with a monochromator and Cu Kα radiation operated at 40 kV and 30 mA was used for record all of the XRD patterns. The diffraction patterns were recorded under the 2-theta range of 0.7 to 5.0 degree with a scan speed of 2 degrees/min and a scan step of 0.02 degree condition. The scattering, the divergent, and the receiving slits were fixed at 0.05 degree, 0.5 degree, and 0.15 mm, respectively.

2.1.2 Surface area analysis

N_2 adsorption–desorption method using a BELSORP, mini-II nitrogen adsorp to meter was used for determining the textural properties of the synthesized materials.

Specific surface areas, pore volumes and pore sizes, and internal and external surface areas were calculated from Brunauer–Emmett–Teller (BET) equation, the Barrett-Joyner-Halanda (BJH) model, and the t-plot equation, respectively.

2.1.3 Fourier transform infrared spectroscopy (FT-IR)

Functional groups present in the synthesized materials were verified by FT-IR technique using the impact 410 (Nicolet) with the transmission mode in the range of 4000-400 cm^{-1}.

2.1.4 Scanning electron microscopy (SEM)

The samples were dispersed in ethanol and dropped on carbon sticky tape mounted on sample holders and coated the samples with gold. Then, morphology and particle sizes of the materials were recorded by JSM-6480LV (JEOL) scanning electron microscope instrument.

2.1.5 Transmission electron microscopy (TEM)

The prepared samples were dispersed in ethanol and dropped on copper grid follow by performed on JEM-2100 (JOEL) transmission electron microscope to study the mesoporous channels and particles sizes of the prepared mesoporous materials.

2.1.6 Acid-base back titration

2.1.6.1 Acid back titration

2.1.6.1.1 Standardization of HCl with Na_2CO_3

The Na_2CO_3 solution was prepared by dissolving of 0.02 g Na_2CO_3 in deionized water. The volume of the solution was then adjusted to 50.00 mL using a volumetric flask. After that, 10.00 mL of the prepared Na_2CO_3 solution was titrated with 0.005 M HCl using methyl orange as an indicator.

2.1.6.1.2 Titration of the prepared catalysts with HCl

The acid capacities of the prepared catalysts were examined according to a previous report [56] with some modifications. Briefly, 0.05 g of each catalyst and 20 mL of 0.005 M NaOH solution were added to a conical flask. After 1 h of reaction at room temperature of stirring, the mixture was filtered and rinsed repeatedly for four times with deionized water. Then, titration between the filtrate and 0.005 M HCl by using phenolphthalein as an indicator was studied.

2.1.6.2 Base back titration

2.1.6.2.1 Standardization of NaOH with KHP

The solution of KHP was prepared by dissolving of 0.05 g of KHP in deionized water and then volume of the solution was adjusted to 50.00 mL using a volumetric flask, followed by titration of 10.00 mL of the prepared KHP solution with 0.005X M NaOH using phenolphthalein as an indicator.

2.1.6.2.2 Titration of the synthesized catalysts with NaOH

The base capacities of the prepared catalysts were examined according to a previous report [56] with some modifications. Briefly, 0.05 g of each catalyst and 20 mL of 0.005 M HCl solution were added to a conical flask. After 1 h of reaction at room temperature for stirring, the mixture was filtered and rinsed repeatedly for four times with deionized water. Then, titration between the filtrate and 0.005 M HCl by using phenolphthalein as an indicator was studied.

2.1.7 Thermogravimetric analysis (TGA)

The thermal stability of the synthesized materials was determined by the SDT Q600 instrument under air flow of 400 mL min^{-1} with the heating rate of 10 $^{o}C\ min^{-1}$.

2.1.8 X-ray photoelectron spectroscopy (XPS)

An AMICUS photoelectron spectrometer equipped with an Mg Kα X-ray as a primary excitation source and KRATOS VISION2 software was used for the determination of the –SH and $–SO_3H$ groups in the synthesized mesoporous materials.

2.1.9 Inductively coupled plasma optical emission spectrometer (ICP-OES)

Pd contents in trifunctional synthesized materials were measured using ICP-OES (Perkin Elmer Optima 2100).

2.1.10 Nuclear magnetic resonance (NMR)

Varian Mercury NMR spectrometer (Varian, USA) at 400 MHz and 100 MHz was used to recorded ^{1}H-NMR and ^{13}C-NMR spectra, respectively.

2.1.11 Gas chromatography (GC)

The resultant solutions from the one-pot deacetylation-aldol reaction of benzaldehydedimethylacetal with malononitrile were analyzed by a Varian CP-3800 gas chromatograph equipped with a flame ionization detector (FID) and a 30 m length x 0.32 mm HP-5 column with a split ratio of 1:50. The maximum temperature

of the HP-5 column was 325 ^{o}C. For the measurement, 1 μL of a sample was injected into the HP-5 column using the temperature program described in Table 2.1.

Table 2.1 The GC temperature program for product analysis

Temperature (^{o}C)	Rate (^{o}C min^{-1})	Hold (min)
60	-	3
315	25	5

2.2 Chemicals

Table 2.2 List of chemicals

Chemicals	Supplier
Cetyltrimethylammoniumbromide (CTAB)	Aldrich
Tetraethylorthosilicate (TEOS)	Aldrich
(3-amino- propyl) triethoxysilane (APTES, N)	Aldrich
3-(trimethoxysilylpropyl) diethylenetriamine (DETTMS, NNN)	Aldrich
3-mercapto- propyltrimethoxysilane (MPTMS)	Aldrich
Ethyl trans-α-cyanocinnamate ($C_{12}H_{11}NO_2$)	Aldrich
3-(2-Aminoethylamino) propyltrimethoxysilane (AAPTMS, NN)	Alfa Aesar
Acetic acid (CH_3COOH)	Merck
Sodium hydroxide (NaOH)	Merck
Hydrogen peroxide (30%) solution (H_2O_2)	Merck
Hydrochloric acid (HCl)	Merck
Methanol (CH_3OH)	Merck
Potassium hydrogen phthalate (KHP)	Merck
Ethylcyanoacetate ($C_5H_7NO_2$)	Merck
Diethylmalonate ($C_7H_{12}O_4$)	Merck

Benzaldehydedimethylacetal (**A**)	Sigma-Aldrich
Benzaldehyde (**B**)	Sigma-Aldrich
Benzylidene malononitrile (**C**)	Sigma-Aldrich
p-xylene (C_8H_{10})	Sigma-Aldrich
Malononitrile ($C_3H_2N_2$)	Sigma-Aldrich
Sodium sulfate (Na_2SO_4)	Sigma-Aldrich
Dimethylmalonate ($C_5H_8O_4$)	Sigma-Aldrich
5% Pd/Al_2O_3 (commercial)	Sigma-Aldrich
Diethyl benzylidenemalonate ($C_{14}H_{16}O_4$)	TCI
Sodium carbonate (Na_2CO_3)	UNIVAR
Acetone (C_3H_6O)	RCI Labscan
Toluene ($C_6H_5CH_3$)	RCI Labscan

Solvents such as hexane and EtOAc for extraction and chromatography were commercial grade. Merck silica gel 60 (70-230 mesh) was operated for column chromatography. Silica gel plates (Merck F245) was used for thin layer chromatography (TLC).

2.3 Preparation of catalysts

2.3.1 Synthesis of acid-base SA_2N_2 catalyst

The bifunctional acid-base SA_2N_2 catalyst was prepared through a co-condensation method which described by Huang et al [57] to functionalize the internal surface of mesoporous silica with acid groups and subsequent functionalize the external surface with the base groups. Briefly, the solution of CTAB was prepared by dissolving of 4 g of CTAB in 960 mL of H_2O and 14 mL of 2 M NaOH. Then, 20 mL of TEOS was added dropwise to the above solution under continuous stirring for 1 h at 80 $^{\circ}$C. After that, the amount of MPTMS (2 mmol) was added and the mixture was

stirred for an additional 2 h. Finally, the product was filtered, washed with deionized water, and dried at 120 °C overnight. The obtained materials were designated as SH_2-CTAB, where 2 represent the amount (in mmol) of MPTMS. An example of the obtained materials is illustrated in Scheme 2.1.

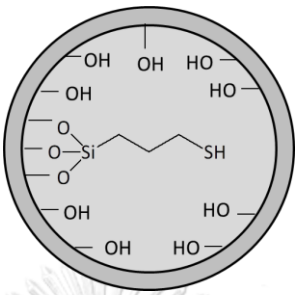

Scheme 2.1 The internal surface of mesoporous silica functionalized with MPTMS.

In order to selectively functionalize the external surface of mesoporous silica with APTES through post-synthesis grafting, the as-prepared SH_2-CTAB solid with the CTAB template remained inside mesoporous channels was refluxed in 500 mL of toluene at 120 °C. Then, 2 mmol of APTES was added to the solution and stirred for 6 h. Finally, the product was filtered, washed with toluene, and dried at 120 °C overnight and designated as SH_2N_2-CTAB, where 2 (the subscription of N) represents the amount (in mmol) of APTES. An example of the obtained materials is illustrated in Scheme 2.2.

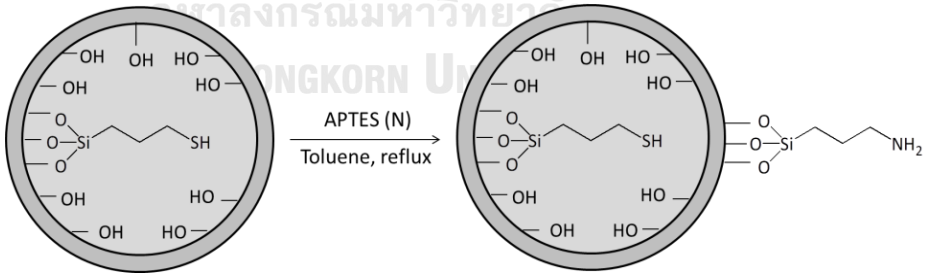

Scheme 2.2 Post-grafting synthesis by functionalizing the external surface of SH_2-CTAB with APTES.

To convert the thiol groups (-SH) to sulfonic acid groups (-SO_3H), the as-prepared SH_2N_2-CTAB material was refluxed in a mixed solution containing 20 mL of gracial acetic acid and 40 mL of 30% H_2O_2 at 100 °C for 6 h. Then, the resultant solid was filtered, washed with deionized water, and dried at 120 °C overnight and

designated as SA_2N_2-CTAB. An example of the obtained materials was illustrated in Scheme 2.3.

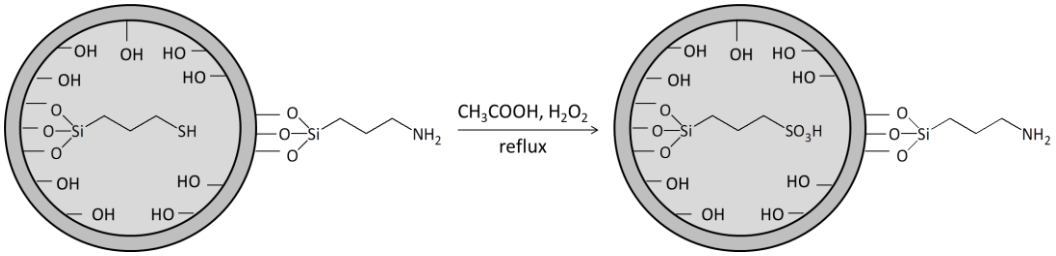

Scheme 2.3 Conversion of thiol groups to sulfonic acid groups.

The CTAB template remained inside the mesopores of the materials was then removed by the extraction method using a mixed solution containing 500 mL of methanol and 5 mL of concentrated HCl at 60 °C for 6 h. Finally, the solid product was filtered, washed with deionized water, and dried at 150 °C overnight. The final product was designated as SA_2N_2. An example for the preparation of SA_2N_2 is illustrated in Scheme 2.4.

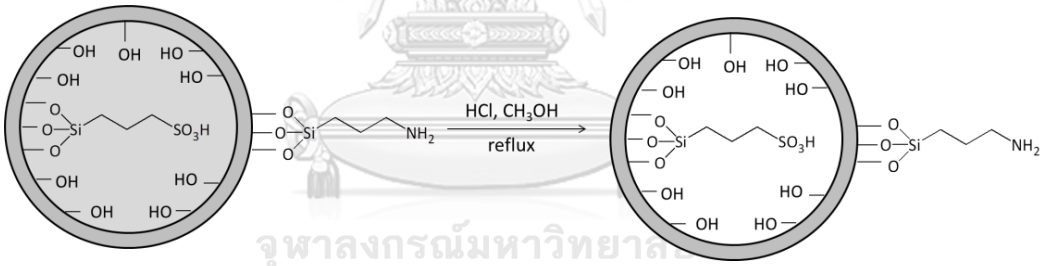

Scheme 2.4 Removal of the CTAB template inside the mesopores of the materials.

2.3.2 Synthesis of acid-base N_2SA_2 catalyst

The bifunctional acid-base N_2SA_2 catalyst was synthesized by functionalizing the internal surface of mesoporous silica with base groups and subsequent functionalizing the external surface with the acid groups. The bifunctional mesoporous material was prepared using the same manner as described in Section 2.3.1, except that APTES was used to replace MPTMS in the co-condensation step and that MPTMS was used to replace APTES in the grafting step. The obtained materials were designated as N_2SA_2. An example for the preparation of N_2SA_2 was illustrated in Scheme 2.5.

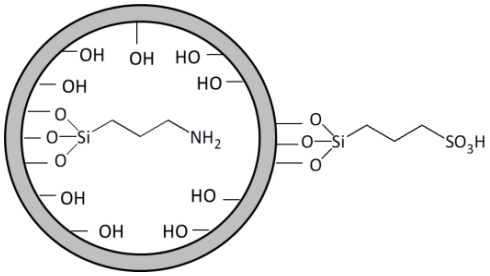

Scheme 2.5 Mesoporous silica containing sulfonic acid groups on the external surface and amine groups on the internal surface.

2.3.3 Synthesis of SA_xN_2 with different acid loadings

SA_xN_2 were prepared using the same manner as described in Section 2.3.1, except that 0.5, 1, and 2 mmol of MPTMS was used. The obtained materials were designated as SA_xN_2, where x = 0.5, 1, and 2 represents the initial loading (in mmol) of MPTMS. The designated names of each material are presented in Table 2.3.

Table 2.3 Designated names of mesoporous silica containing different acid loadings

Materials	Acid loading (mmol)	Base loading (mmol)
$SA_{0.5}N_2$	0.5	2
SA_1N_2	1	2
SA_2N_2	2	2

2.3.4 Synthesis of $SA_{0.5}N_y$ with different base loadings

$SA_{0.5}N_y$ were prepared using the same manner as described in Section 2.3.1 by varying base loading (0.5, 2, and 4 mmol of APTES) and fixed 0.5 mmol of MPTMS. The obtained materials were designated as $SA_{0.5}N_y$, where y = 0.5, 2, and 4 represents the initial loading (in mmol) of APTES. The designated names of each material are presented in Table 2.4.

Table 2.4 Designated names of mesoporous silica containing different base loadings

Materials	Amount of acid (mmol)	Amount of base (mmol)
$SA_{0.5}N_{0.5}$	0.5	0.5
$SA_{0.5}N_2$	0.5	2
$SA_{0.5}N_4$	0.5	4

2.3.5 Synthesis of $SA_{0.5}NN_4$ and $SA_{0.5}NNN_4$

The mesoporous materials containing 0.5 mmol of acid loading and 4 mmol of base loading were synthesized using the same manner as described in Section 2.3.4, except that three types of aminosilanes containing different numbers of amino groups were used:

(i) 3-aminopropyltriethoxysilane (APTES, N) containing one primary amine

(ii) [3-(2-aminoethylamino)propyltrimethoxysilane] (AAPTMS, NN) containing one primary and one secondary amines

(iii) 3-(trimethoxysilylpropyl)diethylenetriamine (DETTMS, NNN) containing one primary and two secondary amines.

The structures of the three amino silanes were shown in Fig 2.1 and the names of each amino silanes are given in Table 2.5.

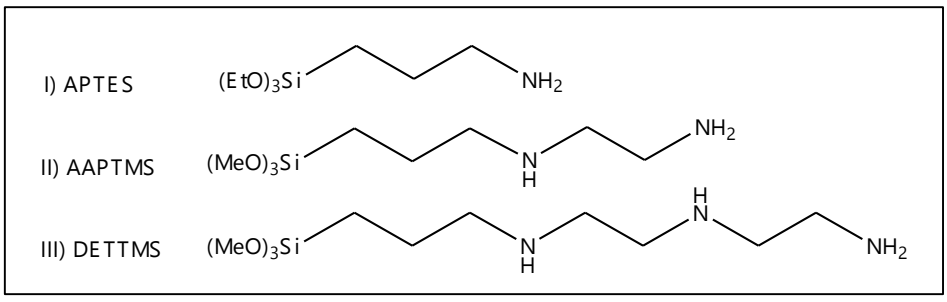

Figure 2.1 Chemical structures of amino-organosilanes.

Table 2.5 Designated names of mesoporous silica containing different numbers of amino groups

Materials	Amount of acid (mmol)	Amount of base (mmol)	Type of base
$SA_{0.5}N_4$	0.5	4	APTES
$SA_{0.5}NN_4$	0.5	4	AAPTMS
$SA_{0.5}NNN_4$	0.5	4	DETTMS

2.4 Catalytic testing of one-pot deacetylation-Knoevenagel reaction using bifunctional catalysts

The procedure for one-pot deacetylation-Knoevenagel reaction of benzaldehydedimethylacetal (**A**) with malononitrile was modified from a previously published article [58]. Briefly, benzaldehydedimethylacetal (0.15 mmol), malononitrile (1.2 mmol), p-xylene (0.5 mmol, internal standard), and each bifunctional catalyst (40 mg) were added in a two-necked round bottom flask equipped with an oil bath, schlenk line, and a magnetic stirring bar under nitrogen atmosphere. The reaction mixture was magnetically stirred at 90 ^{o}C for 0-5 h. After the reaction was stopped, the used catalyst was separated from the reaction mixture by filtration, and the filtrate was analyzed by a Varian CP-3800 gas chromatograph equipped with a flame ionization detector (FID). Conversion of **A**, and yields of products were calculated as follows:

$$\text{Conversion of } \mathbf{A}\ (\%) = \frac{\text{Initial mole of } \mathbf{A} - \text{Final mole of } \mathbf{A}}{\text{Initial mole of } \mathbf{A}} \times 100$$

$$\text{Yield of } \mathbf{B}\ (\%) = \frac{\text{Mole of } \mathbf{B}}{\text{Initial mole of } \mathbf{A}} \times 100$$

$$\text{Yield of } \mathbf{C}\ (\%) = \frac{\text{Mole of } \mathbf{C}}{\text{Initial mole of } \mathbf{A}} \times 100$$

2.5 Catalytic testing of other one-pot deacetylation-condensation reactions

The reaction was performed using the same procedure as described in Section 2.4, except that ethyl cyanoacetate or diethylmalonate was used to replace malononitrile.

2.6 Reusability of catalysts

The reusability of catalyst was modified from a reported literature [5]. After it reaction, the catalyst was recovereddfrom the reaction by centrifugation and washed with acetone and dried at 120 $^{\circ}$C for 24 h.

2.7 Effect of reaction set-up systems

The reactants were carried out using the same procedure as described in Section 2.4, except that the reaction was performed in a Parr reactor under 10 bar of N_2 pressure.

2.8 Synthesis of benzylmalononitrile (D)

The procedure for synthesis of benzylmalononitrile (**D**) was carried out in a 100 mL Parr reactor. Briefly, the reaction was performed by adding benzylidenemalononitrile (**C**, 200 mg), p-xylene (0.5 mmol, internal standard), catalyst (5% Pd/Al_2O_3 (commercial), 100 mg), and 15 mL of toluene in the reactor. The reactor was purged with H_2 three times to remove air and then the reactor was closed, stirred and heated at 90 ℃ for 5 h under 10 bar of H_2 atmosphere. After the reaction was terminated, the used catalyst was separated by filtration, and the product **D** was then extracted with ethyl acetate (30 mL) and deionized water for three times. The combined organic extracts were dried using anhydrous Na_2SO_4. After evaporation under vacuum, the residue was purified by column chromatography (hexane:ethyl acetate = 3:1) to afford product **D**.

2.9 Loading of Pd nanoparticles into $SA_{0.5}N_4$

The trifunctional acid-base-metal catalyst was prepared by the impregnation method described by Biradar et al. [50]. The $SA_{0.5}N_4$ material (200 mg) was dispersed in 80 ml of distilled water via sonication. After that, Pd(II) solution (0.03, 0.2, and 1 wt.%) was slowly added to the reaction mixture and then stirred at room temperature for 30 min to let Pd(II) ions anchor onto the NH_2 groups of $SA_{0.5}N_4$. Then, 1000 µL of 1 M $NaBH_4$ solution was added. The color of solution was changed from yellowish to black, indicating that the transformation of the Pd(II) ions to Pd(0). The solid material was separated by filtration, washed with deionized water, and dried at 120 °C overnight. The final product contained organosulphonic acids, amines and Pd nanoparticles co-functionalized on the mesoporous material, or the trifunctional catalyst denoted as $SA_{0.5}N_4Pd_z$, where z = 0.03, 0.2, and 1 represents the initial loading (wt.%) of aqueous solution of $PdCl_2$. An example for the preparation of $SA_{0.5}N_4Pd_z$ is illustrated in Scheme 2.6.

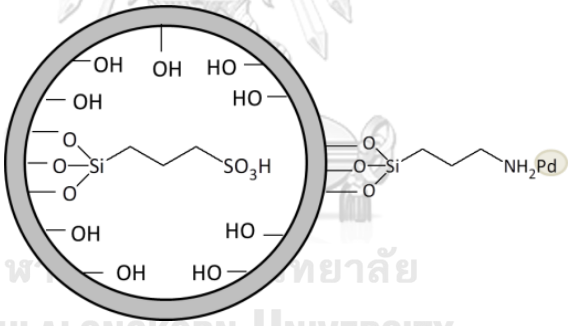

Scheme 2.6 Loading of Pd nanoparticles into $SA_{0.5}N_4$.

2.10 Catalytic testing of one-pot deacetylation-aldol-hydrogenation reaction using trifunctional catalysts

The procedure for one-pot deacetylation-Knoevenagel-hydrogenation reaction was developed from a literature [3]. The reaction was carried out in a 100 mL Parr reactor. In general, the reaction was performed by adding benzaldehydedimethylacetal (**A**) (0.15 mmol), malononitrile (1.2 mmol), p-xylene (0.5 mmol, internal standard), catalyst ($SA_{0.5}N_4Pd_z$ 40 mg, where z = 0.03, 0.2, and 1 represents the initial loading (wt.%) of aqueous solution of $PdCl_2$), and 15 mL of

toluene in the reactor. The reactor was purged with H_2 three times to remove air and then the reactor was closed, stirred and heated at 90 ℃ for 5 h under 10 bar of H_2 atmosphere. After the reaction was stopped, the remaining H_2 was removed by a careful venting process. The used catalyst was separated from the reaction mixture by filtration, and the filtrate was analyzed by a Varian CP-3800 gas chromatograph equipped with a flame ionization detector (FID). Conversion of **A**, and yields of product (**B** and **C**) were calculated as described in Section 2.4, except that the area percent of **D** was calculated from area percent method [59] as follows :

$$\text{Area percent of } \mathbf{D}\ (\%) = \frac{\text{Area of } \mathbf{D}}{\text{Total area}} \times 100$$

2.11 Factors affecting the yield of product D

2.11.1 Effect of Pd loading

The amount of Pd loading was varied from 0.03-1 wt.% of the $SA_{0.5}N_4Pd_z$ catalyst with the hydrogen pressure of 10 bar for 5 h.

2.11.2 Effect of reaction time

The reaction time was in the range of 5-10 h with the hydrogen pressure of 10 bar and $SA_{0.5}N_4Pd_1$ catalyst.

2.11.3 Effect of hydrogen pressure

The hydrogen pressure was varied in the range of 10-30 bar with the reaction time 5 h and $SA_{0.5}N_4Pd_1$ catalyst.

2.11.4 Effect of types of aminosilanes

The effect of types of aminosilanes containing different numbers of amino groups was also studied. Three types of catalysts: $SA_{0.5}N_4Pd_{0.2}$, $SA_{0.5}NN_4Pd_{0.2}$, and $SA_{0.5}NNN_4Pd_{0.2}$ were studied under the hydrogen pressure of 10 bar for 5 h.

2.11.5 Effect of types of gas used in the reaction

The effect of types of gas was also studied. The reaction was performed for 5 h under 10 bar of nitrogen atmosphere, followed by 5 h under 10 bar of hydrogen atmosphere using $SA_{0.5}N_4Pd_{0.2}$ as the catalyst.

2.12 Catalytic testing of one-pot deacetylation-Knoevenagel-hydrogenation reaction using physical mixed catalysts

The reaction was studied using the same procedure as described in Section 2.10, except that physical mixed catalysts: 40 mg of $SA_{0.5}N_4$, $SA_{0.5}NN_4$, or $SA_{0.5}NNN_4$ and 100 mg of 5% Pd/Al_2O_3 (commercial) were used to replace the trifunctional $SA_{0.5}N_4Pd_z$ catalyst. Furthermore, the reaction was performed under N_2 atmosphere for 5 h. After that, the reactor was purged with H_2 three times to remove N_2 and then the reactor was purged with 10 bar of H_2. The reaction mixture was stirred for another 5 h at the same temperature under H_2 atmosphere.

CHAPTER III

RESULTS AND DISCUSSION

3.1 Characterization of the synthesized materials

3.1.1 Powder X-ray diffraction (XRD)

3.1.1.1 The X-ray diffraction patterns of $SH_{0.5}$-CTAB, $SH_{0.5}N_4$-CTAB and $SA_{0.5}$-N_4 materials

The bifunctional mesoporous silica was prepared by a co-condensation method as described by Huang et al. [57] to functionalize the internal surface of the mesoporous silica with the thiol groups ($SH_{0.5}$-CTAB) and subsequently functionalize the external surface with the base groups by a post-synthetic grafting method ($SH_{0.5}N_4$-CTAB). Then, the conversion of the thiol groups to sulfonic acid groups (–SO_3H) and the removal of CTAB template were performed to obtain the acid-base $SA_{0.5}N_4$ catalyst. The X-ray diffraction patterns of $SH_{0.5}$-CTAB, $SH_{0.5}N_4$-CTAB and $SA_{0.5}$-N_4, representing all synthesized materials, are shown in Fig. 3.1. Their XRD patterns showed three peaks at 2θ = 2.0-2.2°, 3.7-3.8° and 4.3-4.4°, corresponding to (100), (110) and (200) reflection planes of hexagonal MCM-41 silica [60], respectively. The XRD result indicates the successful synthesis of the 2D hexagonal mesoporous structure with a space group of P6mm [61]. This information suggests that after all steps of the modification, the crystallographic ordering of the mesopores was retained [62].

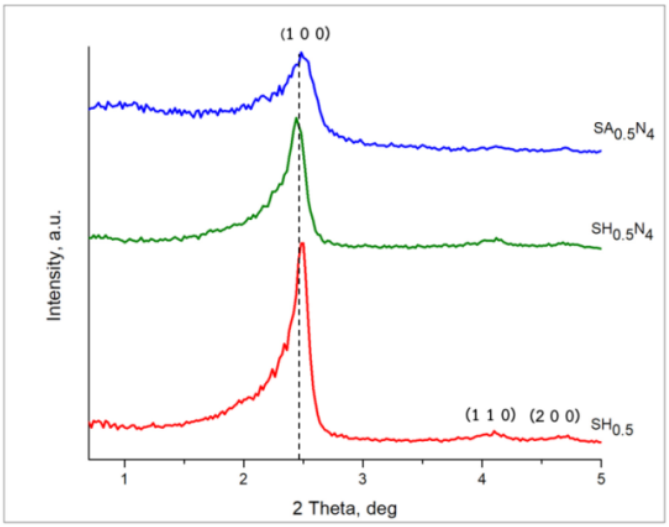

Figure 3.1 XRD patterns of representative synthesized materials: $SH_{0.5}$-CTAB, $SH_{0.5}N_4$-CTAB and $SA_{0.5}N_4$.

3.1.1.2 Powder X-ray diffraction of bifunctional acid-base materials

The XRD patterns of the synthesized acid-base materials containing different acid loadings, base loadings and type of aminoosilane shown in Fig. 3.2. The XRD patterns of the materials with the same acid loading but different base loading: $SA_{0.5}N_{0.5}$, $SA_{0.5}N_2$, and $SA_{0.5}N_4$ were similar except that the decrease in peak intensities was observed when higher base loading used. This observation was probably because the decrease in crystallinity of MCM-41. A similar trend was also observed when the XRD patterns of the materials with the same acid loading but different types of aminosilanes: $SA_{0.5}N_4$, $SA_{0.5}NN_4$, and $SA_{0.5}NNN_4$ were used. It can be explained that when a longer chain of aminosilane was used, the decrease in peak intensity was observed due to the decrease in crystallinity of MCM-41. The XRD results also indicate that the modification of MCM-41 with base loading and type of aminoosilane in this work did not destroy the well-ordered mesoporous structure of MCM-41 [63].

In addition, when the XRD patterns of the materials with the same base loading but different acid loading: $SA_{0.5}N_2$, SA_1N_2, and SA_2N_2 were compared, the peak due to the (1 0 0) plane was slightly shifted to higher angles for

SA_1N_2 and SA_2N_2 samples, relative to that of $SA_{0.5}N_2$. This occurrence was due to a decrease in the *d*-spacing between the crystallographic plane of mesoporous MCM-41 [64]. This result suggests that the addition of a large amount of MPTMS might disturb the self-assembly of surfactant micelles and the silica precursors [65].

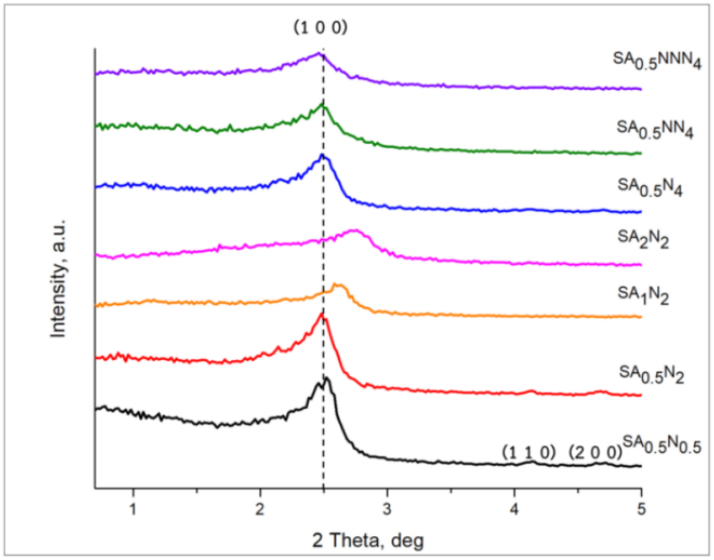

Figure 3.2 XRD patterns of bifunctional acid-base materials.

3.1.2 N_2 adsorption-desorption

N_2 adsorption-desorption technique was used to examine pore characteristics of the synthesized materials. The Brunauer-Emmett-Teller (BET) method was used for calculation of surface areas of the synthesized materials while Barret-Joyner-Halender (BJH) equation were used to calculate pore diameters and pore volumes. Internal and external surface areas were calculated from the t-plot equation. The textural properties of the synthesized materials were listed in Table 3.1. The two acid-base materials with different site isolation: SA_2N_2 (acid on internal surface; base on external surface) and N_2SA_2 (base on internal surface; acid on external surface) were compared. The N_2SA_2 material had a surface area of 686 $m^2 g^{-1}$, a pore diameter of 2.43 nm, and a pore volume of 0.45 $cm^3 g^{-1}$ while those of the SA_2N_2 material were lower: a surface area of 615 $m^2 g^{-1}$, a pore diameter of 2.43 nm, and a pore volume of 0.31 $cm^3 g^{-1}$.

Among the materials with the same base loading but different acid loadings: $SA_{0.5}N_2$, SA_1N_2 and SA_2N_2, $SA_{0.5}N_2$ had the highest surface area of 691 $m^2 g^{-1}$ and the largest pore volume of 0.35 $cm^3 g^{-1}$. In the case of SA_1N_2 and SA_2N_2, their surface areas and pore volumes were decreased to 660 $m^2 g^{-1}$ and 0.32 $cm^3 g^{-1}$ for SA_1N_2; and 615 $m^2 g^{-1}$ and 0.31 $cm^3 g^{-1}$ for SA_2N_2. This could be explained that their mesopore channels were occupied with higher amounts of acid-organic groups. The same trend was also observed for the materials with the same acid loading but different base loading: $SA_{0.5}N_{0.5}$, $SA_{0.5}N_2$ and $SA_{0.5}N_4$. Moreover, when comparing the textural properties of the materials with the same acid loading but different types of base (aminosilane): $SA_{0.5}N_4$, $SA_{0.5}NN_4$, and $SA_{0.5}NNN_4$, the results show that surface area, pore diameter and pore volume were decreased with increasing the chain length of aminosilane. This was likely because longer aminosilanes had a more tendency to block the mesopores, causing the lower surface area, smaller pore diameter and smaller pore volume.

According to the calculation from the t-plot equation, among the materials with the same base loading but different acid loadings: $SA_{0.5}N_2$, SA_1N_2 and SA_2N_2, $SA_{0.5}N_2$ had the highest internal surface area of 599 $m^2 g^{-1}$. In the case of SA_1N_2 and SA_2N_2, their internal surface areas were decreased to 585 $m^2 g^{-1}$ for SA_1N_2; and 535 $m^2 g^{-1}$ for SA_2N_2. This could be explained that most of the acid groups were deposited in the mesopores rather than on the external surface of the support while the external surface remained roughly constant (81-85 $m^2 g^{-1}$). The same trend was also observed for the materials with the same acid loading but different base loading: $SA_{0.5}N_{0.5}$, $SA_{0.5}N_2$ and $SA_{0.5}N_4$, implying that most of the amine groups were deposited in the external surface of the support rather than on the internal surface of the support. Moreover, when comparing the textural properties of the materials with the same acid loading but different types of base (aminosilane): $SA_{0.5}N_4$, $SA_{0.5}NN_4$, and $SA_{0.5}NNN_4$, $SA_{0.5}N_4$ had the highest external surface area of 52 $m^2 g^{-1}$. In the case of SA_1N_2 and SA_2N_2, their external surface areas were decreased to 41 $m^2 g^{-1}$ for $SA_{0.5}NN_4$; and 16 $m^2 g^{-1}$ for $SA_{0.5}NNN_4$. This was likely because most of longer aminosilanes was deposited in the external surface than on the internal surface of the support. This result confirms that the internal surface of mesoporous

silica was functionalized with acid groups while the external surface was functionalized with base groups.

The textural properties of trifunctional materials were listed in Table 3.1. Among the $SA_{0.5}N_4$ materials doped with different wt.% Pd loadings: $SA_{0.5}N_4Pd_{0.03}$, $SA_{0.5}N_4Pd_{0.2}$ and $SA_{0.5}N_4Pd_1$, $SA_{0.5}N_4Pd_{0.03}$ material had the highest surface area of 603 $m^2\ g^{-1}$, the largest pore diameter of 2.02 nm, and the largest pore volume of 0.36 $cm^3\ g^{-1}$. In the case of $SA_{0.5}N_4Pd_{0.2}$ and $SA_{0.5}N_4Pd_1$, their surface areas, pore diameters and pore volumes were decreased to 386 $m^2\ g^{-1}$, 1.96 nm and 0.31 $cm^3\ g^{-1}$ for $SA_{0.5}N_4Pd_{0.2}$; and 318 $m^2\ g^{-1}$, 1.93 nm and 0.25 $cm^3\ g^{-1}$ for $SA_{0.5}N_4Pd_1$. This could be explained that their mesopore channels were occupied with higher amounts of Pd. Furthermore, the textural propertie of 5% Pd/Al_2O_3 commercial material had surface area of 240 $m^2\ g^{-1}$, pore diameter of 12.1 nm, and pore volume of 0.93 $cm^3\ g^{-1}$.

According to the results from N_2 adsorption-desorption and the fact that the sizes of the starting materials and products for one-pot deacetylation-aldol reaction in this study, benzaldehyde dimethyl acetal (**A**), benzaldehyde (**B**), benzylidenemalononitrile (**C**) and benzylmalononitrile (**D**) are 0.24x0.52, 0.24x0.50, 0.28x0.67, and 0.26x0.68 nm^2, respectively, the starting materials are likely to diffuse efficiently to react at the acid sites, base sites, and metallic sites of bi- and trifunctional catalysts in the mesoporous channels.

Table 3.1 Textural properties of the synthesized materials

Materials	BET surface area ($m^2 g^{-1}$)	Internal surface area ($m^2 g^{-1}$)	External surface area ($m^2 g^{-1}$)	Pore diameter (nm)	Pore volume ($cm^3 g^{-1}$)
N_2SA_2	686	613	72	2.43	0.45
$SA_{0.5}N_{0.5}$	729	600	108	2.14	0.38
$SA_{0.5}N_2$	691	599	85	2.05	0.35
SA_1N_2	660	585	82	1.97	0.32
SA_2N_2	615	535	81	2.09	0.31
$SA_{0.5}N_4$	660	609	52	2.09	0.34
$SA_{0.5}NN_4$	646	607	41	2.01	0.32
$SA_{0.5}NNN_4$	609	597	16	1.99	0.30
$SA_{0.5}N_4Pd_{0.03}$	603	560	47	2.02	0.36
$SA_{0.5}N_4Pd_{0.2}$	386	358	35	1.96	0.31
$SA_{0.5}N_4Pd_1$	318	298	14	1.93	0.25
5% Pd/Al_2O_3	240	171	66	12.1	0.93

N_2 sorption isotherms of representative synthesized materials in each step of the systhesis: $SH_{0.5}$-CTAB, $SH_{0.5}N_4$-CTAB and $SA_{0.5}$-N_4 are shown in Fig. 3.3. $SH_{0.5}$-CTAB and $SH_{0.5}N_4$-CTAB showed that the absorbed amount of gas was small at low P/P_0 relative pressure, [66]. When the removal of CTAB template were performed to obtain the acid-base $SA_{0.5}N_4$ catalyst, the loss of condensation steps around P/P_0 = 0.4 was observed. This result confirms that the template was efficiently removed [67].

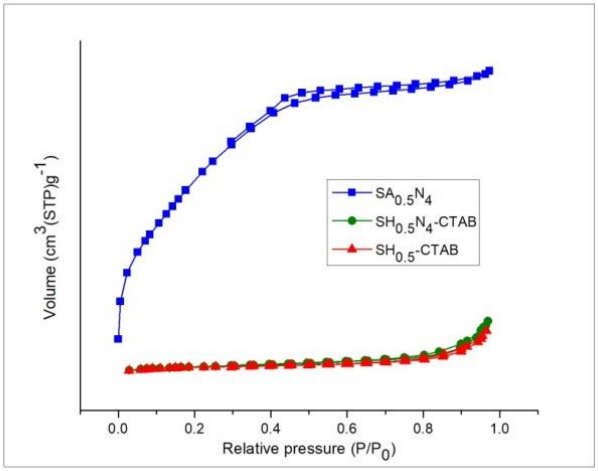

Figure 3.3 N_2 sorption isotherms of representative synthesized materials: $SH_{0.5}$-CTAB, $SH_{0.5}N_4$-CTAB and $SA_{0.5}$-N_4.

Fig. 3.4 shows N_2 sorption isotherms of all synthesized acid-base materials. According to the International Union of Pure and Applied Chemistry (IUPAC) classification [68], all of the isotherms of the synthesized materials were classified as type IV isotherms, a typical characteristic of mesoporous materials. In other words, all of the modification materials showed the structures of mesoporous silica, confirming that the modification of the support with acid and base in this work did not destroy the well-ordered mesoporous structure of MCM-41.

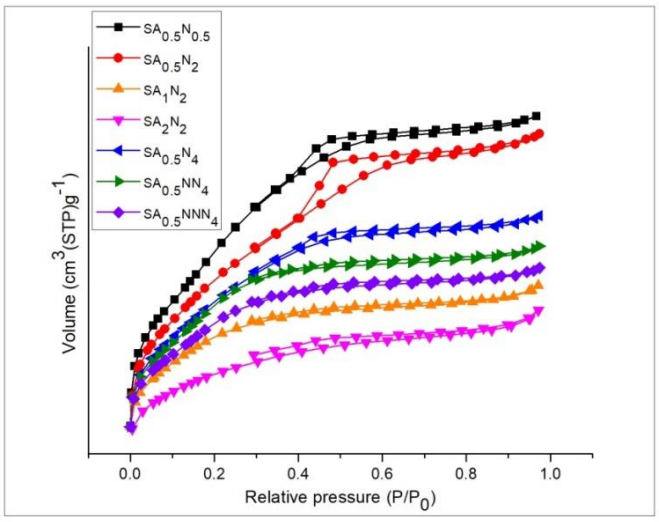

Figure 3.4 N_2 sorption isotherms of bifunctional acid-base materials.

Moreover, N_2 sorption isotherms of trifunctional materials containing different wt.% Pd loadings: $SA_{0.5}N_4Pd_{0.03}$, $SA_{0.5}N_4Pd_{0.2}$ and $SA_{0.5}N_4Pd_1$ are shown in Fig.3.5. After Pd was loaded on $SA_{0.5}N_4$, all of the trifunctional materials were still classified as type IV isotherms, a typical characteristic of mesoporous materials. These results suggest that the modification of the support with acid, base and metal in this work did not destroy the well-ordered mesoporous structure of MCM-41.

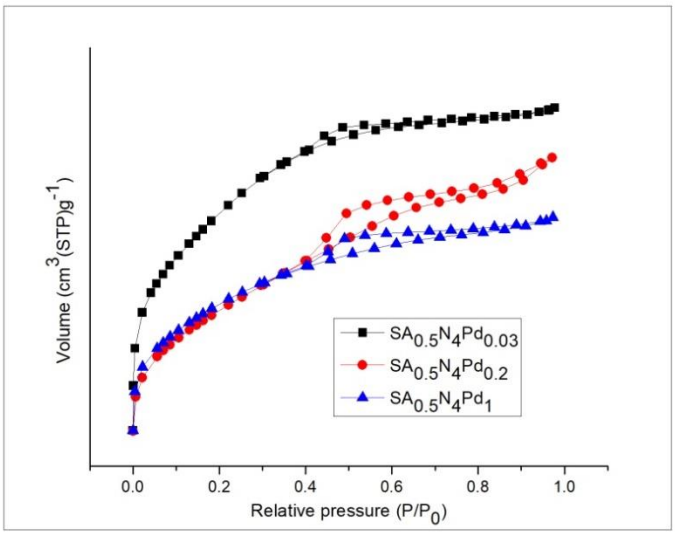

Figure 3.5 N_2 sorption isotherms of trifunctional materials containing different wt.% Pd loadings: $SA_{0.5}N_4Pd_{0.03}$, $SA_{0.5}N_4Pd_{0.2}$ and $SA_{0.5}N_4Pd_1$.

3.1.3 Fourier transform infrared spectroscopy (FT-IR)

The presence of functional groups in the synthesized mesoporous silica supported acid-base catalysts was confirmed by Fourier transform infrared spectroscopy (FT-IR) (Fig. 3.6). Considering the spectrum of $SA_{0.5}N_4$-CTAB, the peaks of the CTAB template due to the C–H stretching and C-H bending vibrations were observed at 2850-3000 and 1460 cm^{-1}, respectively. These peaks disappeared or almost disappeared in the spectra of all acid-base materials, suggesting that the template was efficiently removed after extraction [62]. The peak at 1032 cm^{-1} was assigned to the asymmetric stretching vibration of S=O bands and the peak at 1125 cm^{-1} was assigned to the symmetric vibration of S=O bands. These results confirmed the presence of sulfonic groups in the synthesized materials. In addition, an

absorption of 610 cm^{-1} was also observed, which was attributed to the bending vibration of –OH groups of SO_3H groups [69]. The presence of two peaks at 1536 and 801 cm^{-1} could be attributed to the symmetric N–H stretching band and the N–H out-of-plane bending vibration from the NH_2 group, respectively [70]. These results confirm that the amino groups were grafted on the surface of materials in all samples.

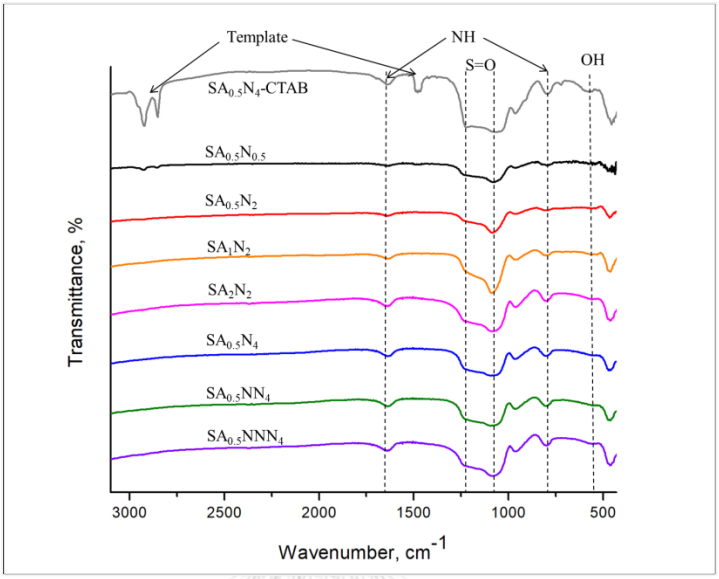

Figure 3.6 FT-IR spectra of the synthesized materials.

3.1.4 Scanning electron microscope (SEM)

The morphologies and sizes of all modified bifunctional materials were measured by SEM as shown in Fig. 3.7. The SEM images of all materials: $SA_{0.5}N_{0.5}$, $SA_{0.5}N_2$, SA_1N_2, SA_2N_2 $SA_{0.5}N_4$, $SA_{0.5}NN_4$ and $SA_{0.5}NNN_4$ were similar. Their structures were small kidney-bean-shaped rods [67] with an average particle size of ~0.8x1.3 μm^2. This observation indicates that the morphologies of the mesoporous materials were preserved after their modification with acid and base.

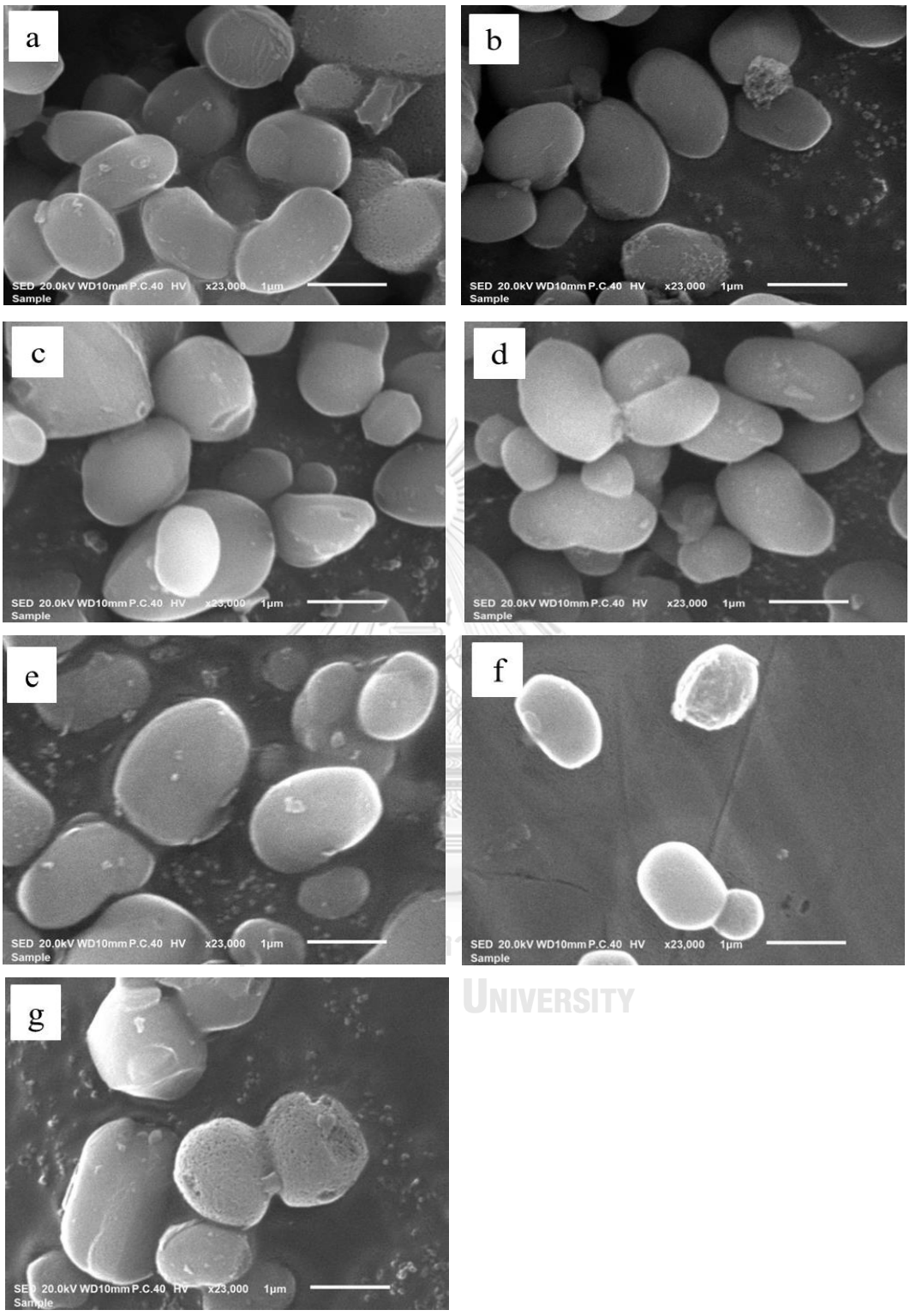

Figure 3.7 SEM images of (a) $SA_{0.5}N_{0.5}$, (b) $SA_{0.5}N_2$, (c) SA_1N_2, (d) SA_2N_2, (e) $SA_{0.5}N_4$, (f) $SA_{0.5}NN_4$ and (g) $SA_{0.5}NNN_4$.

3.1.5 Transmission electron microscope (TEM)

The presence of mesoporous channels of the representative material: $SA_{0.5}N_4$ was determined by TEM as shown in Fig. 3.8. The arrangement of parallel straight channels in a uniform hexagonal structure was found, which could be ascribed to the (1 1 0) and (1 0 0) directions of hexagonal symmetry p6mm phase, respectively [62]. This result confirms the XRD results for the formation of ordered mesoporous structure.

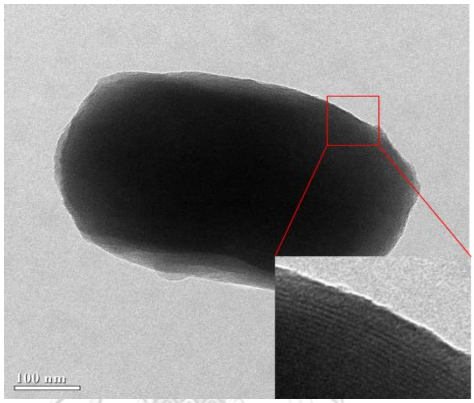

Figure 3.8 TEM image of the representative synthesized material: $SA_{0.5}N_4$.

3.1.6 Acidity and basicity

The concentrations of acid and base loaded in the mesoporous materials were determined using the back titration method and were listed in Table 3.2. The results confirmed the coexistence of acid and base in all samples. The two acid-base materials with different site isolation: SA_2N_2 (acid on internal surface; base on external surface) and N_2SA_2 (base on internal surface; acid on external surface) were compared. The acidity of N_2SA_2 was found to be 1.03 mmol g^{-1} which was slightly lower than that of SA_2N_2 (1.10 mmol g^{-1}) while the amount of base remained roughly constant (~0.4 mmol g^{-1}). By comparing the acid and base concentrations of the materials with the same base loading but different acid loadings: $SA_{0.5}N_2$, SA_1N_2, and SA_2N_2, the acidity of $SA_{0.5}N_2$ was found to be 0.89 mmol g^{-1} which was lower than that of SA_1N_2 (0.96 mmol g^{-1}), and SA_2N_2 (1.10 mmol g^{-1}) while the amount of base remained roughly constant (~0.4 mmol g^{-1}). In case of the acid and base

concentrations of the materials with the same acid loading but different base loadings: $SA_{0.5}N_{0.5}$, $SA_{0.5}N_2$, and $SA_{0.5}N_4$, the basicity of $SA_{0.5}N_4$ was found to be 0.47 mmol g^{-1} which was higher than that of $SA_{0.5}N_{0.5}$ (0.29 mmol g^{-1}), and $SA_{0.5}N_2$ (0.38 mmol g^{-1}) while the amount of acid remained roughly constant (~0.9 mmol g^{-1}). Additionally, when the number of amino groups (aminosilane) was increased in $SA_{0.5}N_4$, $SA_{0.5}NN_4$, and $SA_{0.5}NNN_4$, respectively, the base concentration was also increased: 0.47, 0.50, and 0.57 mmol g^{-1}, respectively. This occurrence might be explained that the increasing of basicity in catalysts resulted from the increasing number of amino groups from aminosilanes.

In addition, the concentrations of acid and base loaded in the trifunctional mesoporous materials were determined. By comparing the acid and base concentrations of the trifunctional materials containing different wt.% Pd loadings: $SA_{0.5}N_4Pd_{0.03}$, $SA_{0.5}N_4Pd_{0.2}$ and $SA_{0.5}N_4Pd_1$, the acidity of $SA_{0.5}N_4Pd_{0.03}$ was found to be 0.80 mmol g^{-1} which was higher than that of $SA_{0.5}N_4Pd_{0.2}$ (0.63 mmol g^{-1}), and $SA_{0.5}N_4Pd_1$ (0.38 mmol g^{-1}). This was likely because some of sulfonic acid groups could anchor Pd nanoparticles [71], causing the lower acidity. Moreover, the basicity of $SA_{0.5}N_4Pd_{0.03}$ was found to be 0.44 mmol g^{-1} which was higher than that of $SA_{0.5}N_4Pd_{0.2}$ (0.28 mmol g^{-1}), and $SA_{0.5}N_4Pd_1$ (0.19 mmol g^{-1}). This occurrence might be explained that the amine groups in the materials could be used to anchor Pd nanoparticles as well [72].

Table 3.2 Acidity and basicity of the synthesized materials

Materials	Acidity (mmol g^{-1})	Basicity (mmol g^{-1})
N_2SA_2	1.03	0.39
$SA_{0.5}N_{0.5}$	0.88	0.29
$SA_{0.5}N_2$	0.89	0.38
SA_1N_2	0.96	0.40
SA_2N_2	1.10	0.42
$SA_{0.5}N_4$	0.89	0.47
$SA_{0.5}NN_4$	0.90	0.50
$SA_{0.5}NNN_4$	0.89	0.57
$SA_{0.5}N_4Pd_{0.03}$	0.80	0.44
$SA_{0.5}N_4Pd_{0.2}$	0.63	0.28
$SA_{0.5}N_4Pd_1$	0.38	0.19

3.1.7 Thermogravimetric analysis (TGA)

The thermal stability of the representative materials: $SA_{0.5}$ and $SA_{0.5}N_4$ was determined using TGA analysis as shown in Fig. 3.9. The results show a weight loss below 100 °C, which was due to the loss of physisorbed water. The weight loss between 200 and 600 °C in both materials was mainly due to the decomposition of the organic groups in the materials [73]. In this temperature range, the weight losses for $SA_{0.5}$, and $SA_{0.5}N_4$ were 21.38 % and 28.75 %, respectively. The greater weight loss of $SA_{0.5}N_4$ was because it contained the higher amount of organic functional groups. Therefore, the result indicates that the incorporation of organic functional groups into the mesoporous materials was successful. Moreover, the result shows that the

bifunctional material was stable at temperature below 200 °C and therefore could be used as a catalyst in a reaction performed at temperature below 200 °C without degradation.

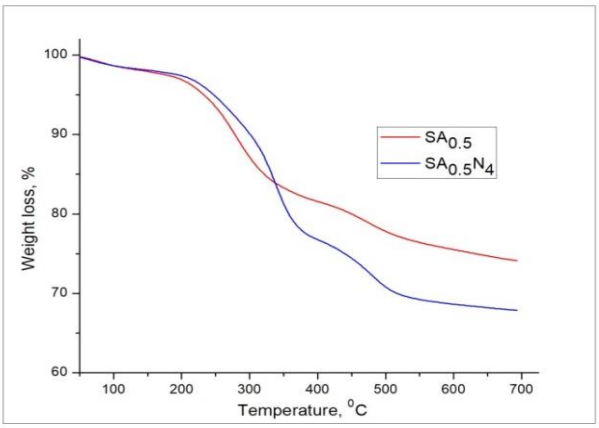

Figure 3.9 TGAs of $SA_{0.5}$ and $SA_{0.5}N_4$.

3.1.8 X-ray photoelectron spectroscopy (XPS)

The determination of the –SH and $–SO_3H$ groups in the representative materials: $SH_{0.5}$ and $SA_{0.5}N_4$ was performed using XPS technique as shown in Fig. 3.10. From the literature reported: the binding energy at 164 eV is S_{2p} electron of the –SH group while that at 169 eV is the sulfonic acid group [74]. This result confirms that using H_2O_2 and acetic acid could convert most of the –SH groups to the SO_3H groups.

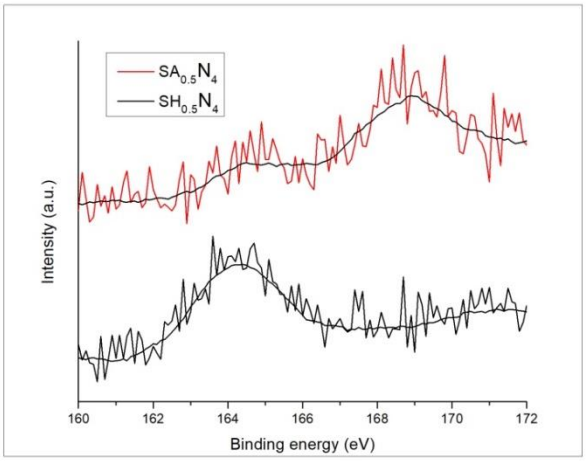

Figure 3.10 XPS spectra of S_{2p} of $SH_{0.5}$ and $SA_{0.5}N_4$.

3.1.9 Inductively coupled plasma optical emission spectrometer (ICP-OES)

Pd contents of trifunctional mesoporous materials were determined using ICP-OES technique and listed in Table 3.3. The results showed that the Pd concentrations were 0.023 ± 0.018, 0.15 ± 0.04 and 0.97 ± 0.09 %w/w in $SA_{0.5}N_4Pd_{0.03,}$ $SA_{0.5}N_4Pd_{0.2}$ and $SA_{0.5}N_4Pd_1$, respectively. This occurrence might be explained that the increase of Pd contents in trifunctional materials resulted from the increasing number of Pd loading. This result confirms that most of Pd used was anchored on the bifunctional mesoporous materials.

Table 3.3 Pd contents in the trifunctional synthesized materials

Materials	Pd (%w/w)
$SA_{0.5}N_4Pd_{0.03}$	0.023 ± 0.018
$SA_{0.5}N_4Pd_{0.2}$	0.15 ± 0.04
$SA_{0.5}N_4Pd_1$	0.97 ± 0.09

3.2 Catalytic activity of the synthesized bifunctional acid-base catalysts

The synthesized bifunctional acid-base mesoporous catalysts were investigated for their catalytic activities in the one-pot deacetalization-Knoevenagel reaction. In this work, the determination of catalytic activities was divided into 6 parts:

(I) Effect of site-separated brønsted acid and base

(II) Effect of acid loading

(III) Effect of base loading

(IV) Effect of aminosilane types

(V) Effect of substrate types

(VI) Reusability of catalysts

The schematic diagram for the one-pot deacetalization-Knoevenagel reaction was shown in Scheme 3.1. Mechanistically, the acid-catalyzed deacetalization of benzaldehydedimethylacetal (**A**) to produce benzaldehyde (**B**) occurred in the first step, followed by the base-catalyzed Knoevenagel condensation of **B** with malononitrile to produce benzylidenemalononitrile (**C**) in the second step.

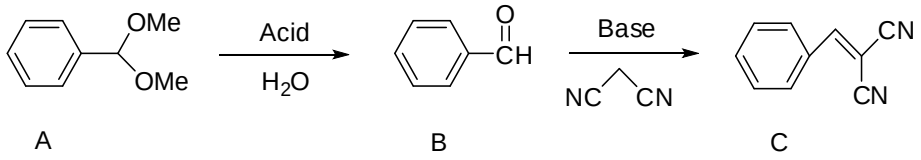

Scheme 3.1 One-pot of deacetylation-Knoevenagel reaction.

3.2.1 Effect of site-separated brønsted acid and base

The two acid-base catalysts with different site isolation: SA_2N_2 (acid on internal surface; base on external surface) and N_2SA_2 (base on internal surface; acid on external surface) were tested for their catalytic activities for the one-pot reaction of **A** with malononitrile under the same conditions: 90 °C, 5 h under nitrogen atmosphere. The catalytic activities including conversion of **A**, yield of **B** and yield of **C** using the synthesized catalysts are listed in Table 3.4. When the reaction was performed using SA_2N_2 (entry 1) and N_2SA_2 (entry 2) catalysts, the results show that, in the first step, two catalysts could completely convert **A** to **B** within 5 h. This finding can be explained by the acidity of the catalysts. The acidity of N_2SA_2 was found to be 1.03 mmol g^{-1} which was similar that of SA_2N_2 (1.10 mmol g^{-1}) and this acid concentration seemed to be high enough for the complete conversion of **A** to **B**. However, in the second step, the yield of **B** using SA_2N_2 was found to be 74.8 % which was lower than the yield of **B** using N_2SA_2 (95.7 %) while yield of **C** using SA_2N_2 was found to be 25.2 % which was higher than the yield of **C** using N_2SA_2 (4.2 %). This observation suggests that, in terms of the yield of **C**, the catalytic performance of SA_2N_2 was more efficient than that of N_2SA_2. In other words, the catalyst having acid sites on the internal surface and the basic sites on the external surface exhibited higher catalytic activity. Moreover, the inner-outer structure separated the acid and basic sites [75]. As shown in Fig. 3.11, the starting materials first passed the outer

shell to the inner core. In this process, **A** was converted to **B**. Then **B** diffuses past the basic sites at the outer to generate **C**. In comparison, the core-shell structure with basic sites at the core and acid sites at the shell designed by Yang et al. could catalyze the deacetalization–Henry cascade reaction (nitromethane was used to replace malononitrile), although the catalyst could convert **A** to **B** in 100% conversion, it took a longer period of time (22 h) for the reaction to complete [76].

The reaction mechanism of the one-pot process on the catalyst surface studied in this work was modified from Rana et al [74] as shown in Scheme 3.2. The cascade reaction was initiated by acidic sites (-SO_3H) on the catalyst to convert benzaldehydedimethyl acetal (**A**) to benzaldehyde (**B**) as shown in Step A1 to A5. After that, the –NH_2 groups on the catalyst acted as nucleophiles and attacked the carbonyl carbon (B1) and in the consequent step water was removed, resulting in the formation of imine intermediate (B4). In the last step, the activated malononitrile reacted with the intermediate (B5), resulting in the formation of benzylidene malononitrile (**C**) and regeneration of amine groups on the surface of the catalyst (B6). According to a previous report by Mu et al., the obtained **B** was further activated by sulfonic acid as shown in B2-B3 steps [77]. For this reason, the presence of sulfonic group was very significant for this reaction. Therefore, in summary, sulfonic acid and amino groups performed a synergetic effect on this one-pot reaction.

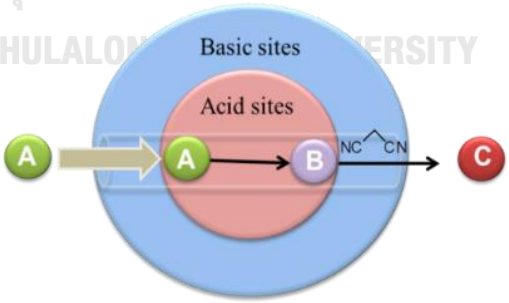

Figure 3.11 Reaction flow of the two-step cascade reaction on the inner-outer structure of bifunctional SA_2N_2 catalyst.

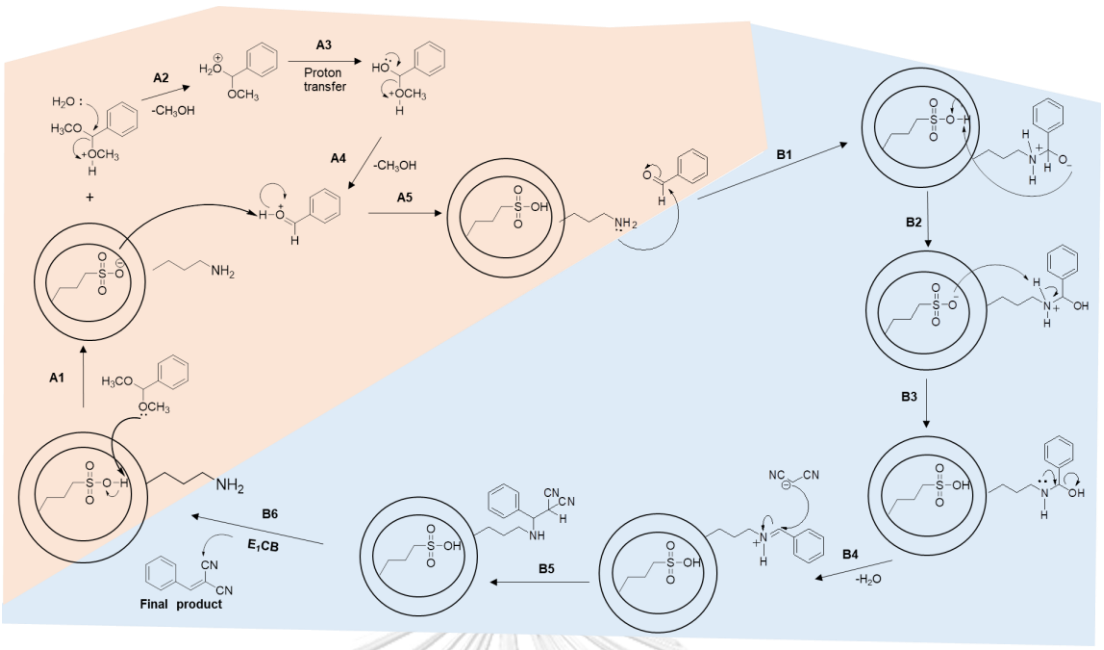

Scheme 3.2 Proposed mechanism of one-pot deacetalization–Knoevenagel reaction.

In addition, monofunctional catalysts with similar inner–outer structures: SA_2 or N_2 (Table 3.4, entries 3 and 4), were tested and the results show that the desired product **C** was not obtained, suggesting that the synthesized materials are ones of efficient catalysts for one-pot cascade reactions requiring both acid and base active species.

Based on the catalytic activity of the synthesized bifunctional catalysts tested in this section, the most effective catalyst was SA_2N_2 (acid on internal surface; base on external surface). Therefore, it was chosen for further studies.

Table 3.4 Catalytic activities of mono- and bifunctional catalysts

Entry	Materials	Conversion of A (%)	Yield of B (%)	Yield of C (%)
1	SA_2N_2	100	74.8	25.2
2	N_2SA_2	100	95.7	4.2
3	SA_2	100	100	N.A.
4	N_2	N.A.	N.A.	N.A.

3.2.2 Effect of acid loading

Three catalysts containing different acid loadings (0.5, 1 and 2 mmol) with fixed base loading (2 mmol): $SA_{0.5}N_2$, SA_1N_2, and SA_2N_2 were tested to compare their bifunctional activity for the one-pot reaction of **A** with malononitrile using the reaction conditions as follows: 90 °C and 0-5 h. The results show that, in the first step, all catalysts could convert **A** to **B** in 100% conversion within 5 h (Fig. 3.12a). However, it was found that SA_2N_2 could completely convert **A** within 0.5 h while the conversion of **A** using $SA_{0.5}N_2$ and SA_1N_2 gradually increased and took about 4 h to reach 100% conversion. This finding can be explained by the acidity of the catalysts. Specifically, the acidity of SA_2N_2 (1.10 mmol g^{-1}) was higher than that of SA_1N_2 (0.96 mmol g^{-1}) and $SA_{0.5}N_2$ (0.89 mmol g^{-1}), leading to a higher rate for the conversion of **A**.

Meanwhile, the yield of **B** was also investigated (Fig. 3.12b). The result suggests that in the cases of $SA_{0.5}N_2$ and SA_1N_2, the yield of **B** gradually increased in the first 4 h before slightly decreasing in the last hour while SA_2N_2 could produce **B** in nearly 100% yield within 0.5 h before slowly decreasing.

In addition, the yield of **C** was also determined as shown in Fig. 3.12c. For all catalysts, the yield of **C** gradually increased during the 5 h reaction time. However, it was observed that the reactivity of SA_2N_2 to produce **C** was poorer than the other two catalysts probably because a higher density of **B** (~80%) inside the pores could not rapidly diffuse to react with the amine groups outside the pore to produce **C**. This finding was supported by the lowest surface area of SA_2N_2 (615 $m^2 g^{-1}$), which was lower than that of SA_1N_2 (660 $m^2 g^{-1}$), and $SA_{0.5}N_2$ (691 $m^2 g^{-1}$), respectively. Therefore, based on the above reasons, 0.5 mmol of acid loading was chosen for further studies.

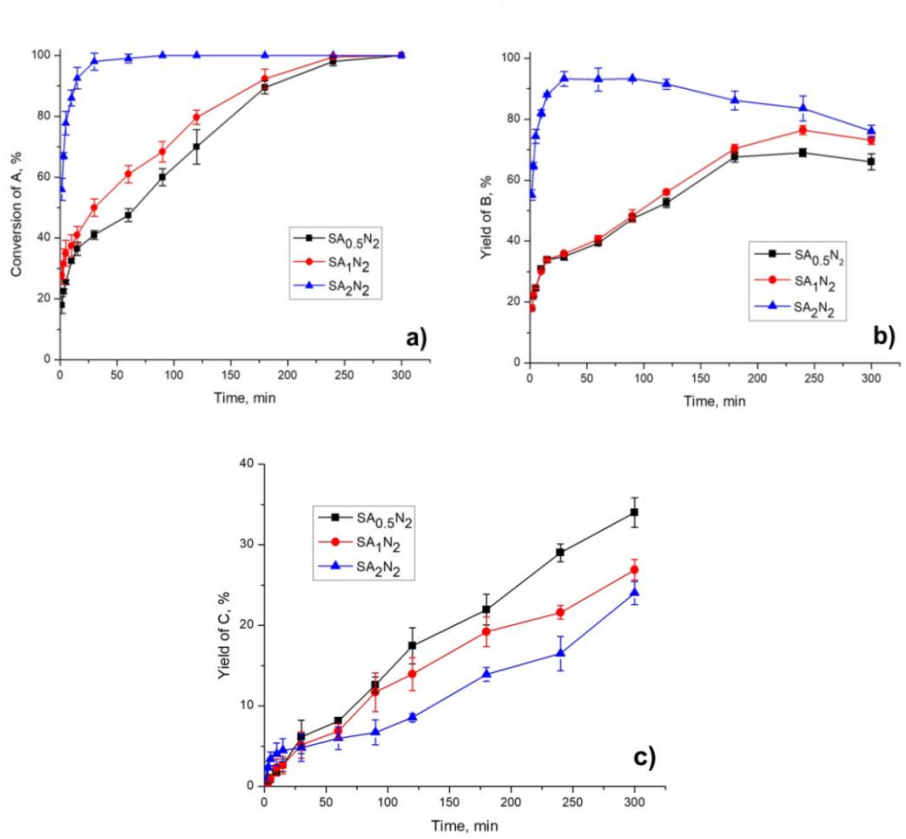

Figure 3.12 Effect of acid loading in catalysts for the one-pot reaction of **A** with malononitrile. (a) conversion of **A**, (b) yield of **B**, (c) yield of **C**. Conditions: 90 °C and 0-5 h.

3.2.3 Effect of base loading

Three catalysts containing different base loadings (0.5, 2 and 4 mmol) with fixed acid loading (0.5 mmol): $SA_{0.5}N_{0.5}$, $SA_{0.5}N_2$ and $SA_{0.5}N_4$ were tested to compare their activity for the one-pot reaction of **A** with malononitrile using the reaction conditions as follows: 90 °C and 0-5 h. The results show that, in the first step, all catalysts could completely convert **A** to **B** within 5 h (Fig. 3.13a). This could be explained by the similar amount of acidity (~0.9 mmol g^{-1}) of each catalyst.

Meanwhile, the yield of **B** was also investigated (Fig. 3.13b). The result suggests that in the cases of $SA_{0.5}N_2$ and $SA_{0.5}N_4$, the yield of **B** gradually increased in the first 3 h before slightly decreasing in the last 2 h while the yield of **B** using $SA_{0.5}N_{0.5}$ gradually increased with time (0-5 h).

In addition, the yield of **C** was also determined as shown in Fig. 3.13c. For all catalysts, the yield of **C** gradually increased during the 5 h reaction time. However, it was observed that the reactivity of $SA_{0.5}N_4$ to produce **C** was higher than those of the other two catalysts probably due to the basicity of the catalysts. Specifically, the basicity of $SA_{0.5}N_4$ (0.47 mmol g^{-1}) was higher than that of $SA_{0.5}N_2$ (0.38 mmol g^{-1}) and $SA_{0.5}N_{0.5}$ (0.29 mmol g^{-1}), leading to a higher yield of **C**. Therefore, based on the above reasons, 4 mmol of base loading was chosen for further studies.

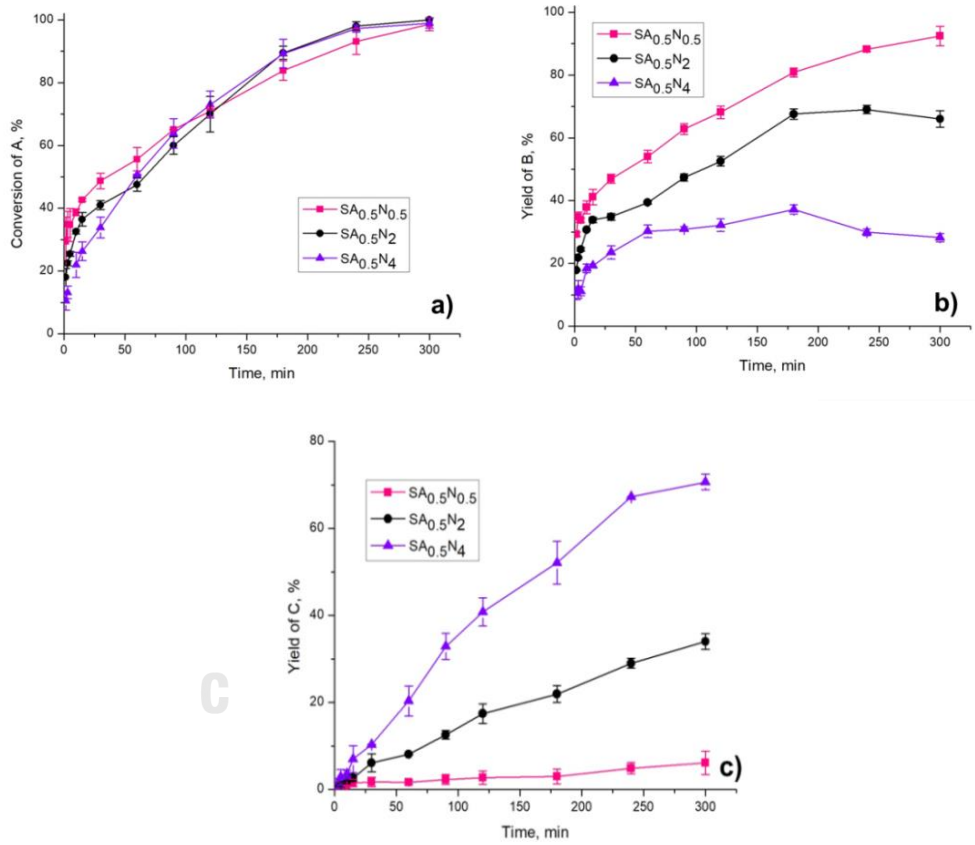

Figure 3.13 Effect of base loading in catalysts for the one-pot reaction of **A** with malononitrile. (a) conversion of **A**, (b) yield of **B**, (c) yield of **C**. Conditions: 90 °C and 0-5 h.

3.2.4 Effect of aminosilane types

The effect of aminosilanes was investigated by using three types of aminosilanes with different numbers of amino groups. The conversion of **A** and the

yield of products are shown in Fig. 3.14. In the first step, when the number of amino groups was increased from one (N) to three (NNN), all catalysts could convert **A** to **B** in a similar trend. The conversion of **A** was completed within 5 h as shown in Fig. 3.14a. This could be explained by the similar amount of acidity (~0.9 mmol g^{-1}) of each catalyst. The intermediate **B** was also monitored as shown in Fig. 3.14b. For all catalysts, yield of **B** were gradually increased when the reaction time was increased. However, the yield of **B** using $SA_{0.5}N_4$ was slowly decreased after the first 3 h of reaction time probably because it could easily diffuse to react with amine functional groups outside the pores. This result was confirmed by the largest surface area of $SA_{0.5}N_4$ (660 m^2 g^{-1}), which was higher than that of $SA_{0.5}NN_4$ (646 m^2 g^{-1}), and $SA_{0.5}NNN_4$ (609 m^2 g^{-1}). In the second step, yield of **C** was determined as shown in Fig. 3.14c. The results show that the yields of **C** were gradually increased when the reaction time was increased for all catalysts used. Interestingly, $SA_{0.5}N_4$ exhibited a higher reactivity than the other two catalysts because it contained the smallest aminosilane molecules, which were less steric hindrance in the reaction to form **C** [78]. Therefore, the catalytic performance of $SA_{0.5}N_4$ was better than $SA_{0.5}NN_4$ and $SA_{0.5}NNN_4$.

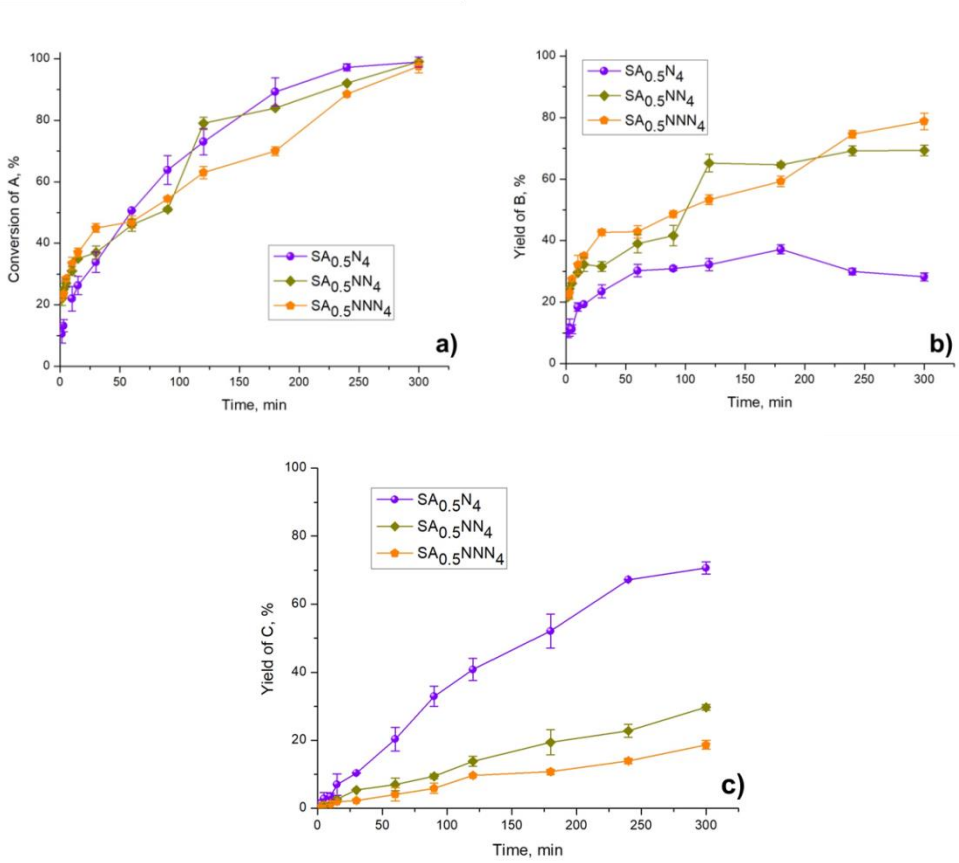

Figure 3.14 Effect of aminosilane types for the one-pot reaction of **A** with malononitrile. (a) conversion of **A**, (b) yield of **B**, (c) yield of **C**. Conditions: 90 °C and 0-5 h.

3.2.5 Effect of substrate types

3.2.5.1 Substitution of malononitrile with ethyl cyanoacetate

The substitution of malononitrile with ethyl cyanoacetate in the one-pot deacetalization-Knoevenagel reaction was investigated and the results are shown in Scheme 3.3. The conversion of **A** and the yield of products are shown in Fig. 3.15. The $SA_{0.5}N_4$ catalyst was used to test the one-pot reaction of **A** with ethyl cyanoacetate using the reaction conditions as follows: 90 °C and 0-5 h. The results show that, in the first step, $SA_{0.5}N_4$ could convert **A** to **B** in 100% conversion within 5 h. In addition, yield of **B** was also investigated. The result suggests that the yield of **B**

gradually increased in the first 1 h before significantly decreased in the last 4 h. In the second step, yield of **C_2** was observed. The yield of **C_2** gradually increased during the 5 h reaction time. Under the 5 h reaction time at 90 °C, the reaction gave 63% yield of the final product. Therefore, based on the above reasons, the one-pot deacetalization-Knoevenagel reaction by substitution of malononitrile with ethyl cyanoacetate was successful by using the $SA_{0.5}N_4$ catalyst.

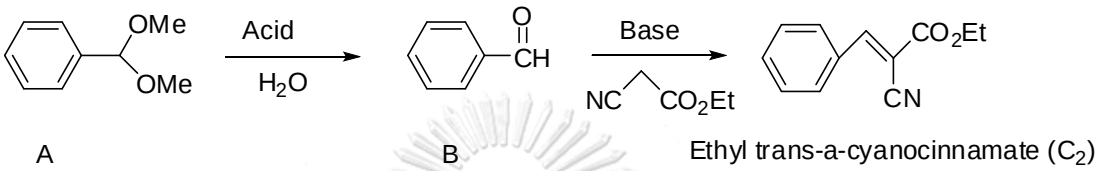

Scheme 3.3 One-pot of deacetylation-Knoevenagel reaction by substitution of malononitrile with ethyl cyanoacetate.

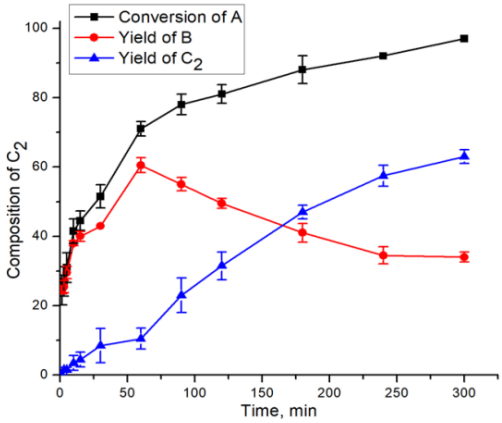

Figure 3.15 The one-pot reaction of **A** with ethyl cyanoacetate. (a) conversion of **A**, (b) yield of **B**, (c) yield of **C_2**. Conditions: 90 °C and 0-5 h.

3.2.5.2 Substitution of malononitrile with diethyl malonate

The substitution of malononitrile with diethyl malonate in the one-pot deacetalization-Knoevenagel reaction was investigated using $SA_{0.5}N_4$ as the catalyst and the results are shown in Scheme 3.4. The conversion of **A** and the yield of products are shown in Fig. 3.16. Conversion of **A** and yield of **B** were gradually

increased when the reaction time was increased while the yield of **C_3** was quite low (less than 15%). As compared to the results from Section 3.2.4 and 3.2.5.1 where the substrates were malononitrile and ethyl cyanoacetate, it was found that the yield of final product by using malononitrile was found to be 70.7 % which was higher than that by using ethyl cyanoacetate (63.0 %) and diethylmalonate (12.2 %). The pK_a values of active methylene compounds: malononitrile, ethyl cyanoacetate and diethylmalonate were reported in Table 3.5. Their pK_a values are in the range of 11.1-16.4. Specifically, the pKa value of malononitrile (11.1) was lower than that of ethyl cyanoacetate (13.1) and diethylmalonate (16.4). The lower pKa of an acid means that it is a stronger acid and has a more efficient ability to donate protons [79]. In other words, the acid with lower pKa led to the formation of a more active methylene compound (carbanion nucleophile) to react with the intermediate in step B5 (malononitrile > ethyl cyanoacetate > diethylmalonate) as shown in the reaction mechanism of the one-pot process (Scheme 2). Consequently, the highest yield of the final product was observed from the reaction with malononitrile.

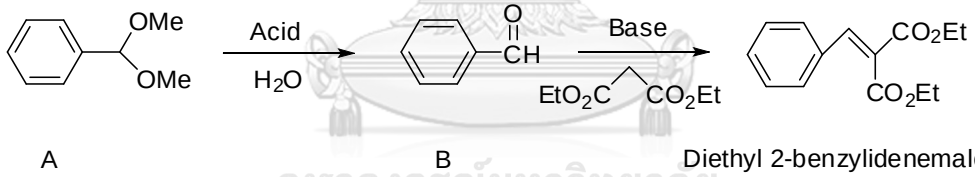

Scheme 3.4 One-pot of deacetylation-Knoevenagel reaction by substitution of malononitrile with diethyl malonate.

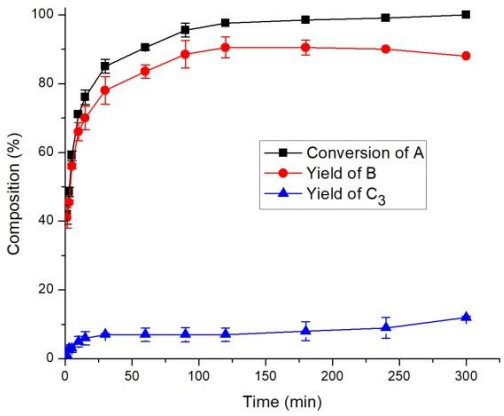

Figure 3.16 The one-pot reaction of **A** with diethylmalonate. (a) conversion of **A**, (b) yield of **B**, (c) yield of **C**. Conditions: 90 °C and 0-5 h.

Table 3.5 pK_a of the substrate types in the one-pot deacetalization-Knoevenagel reaction [80]

Entry	Methylene compounds	pK_a in DMSO
1	Malononitrile	11.1
2	Ethylcyanoacetate	13.1
3	Diethylmalonate	16.4

3.2.6 Reusability of catalysts

For applications of heterogeneous catalysts, the reusability of the catalysts is an important factor to investigate. Based on the above results, the $SA_{0.5}N_4$ catalyst showed the highest catalytic activity in this study. Therefore, $SA_{0.5}N_4$ was chosen for catalyst reusability test. Staring with the recovery of catalyst by using centrifugation, then washed with ethanol, and reused in the next run. As shown in Fig. 3.17, the results prove that the catalyst could be reused for at least four times without a significant decrease in activity, suggesting that the bifunctional acid and base groups were strong covalent-bonded on the surface of the mesoporous support.

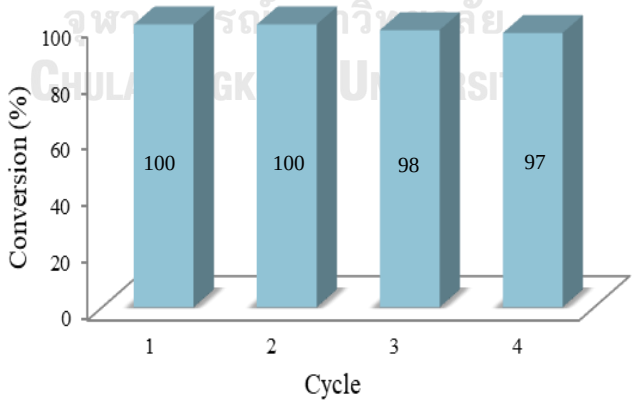

Figure 3.17 Reusability test using $SA_{0.5}N_4$ catalyst.

3.2.7 Effect of reaction set-up systems

The catalytic activity of the synthesized acid-base catalysts in the one-pot deacetalization-Knoevenagel reaction using two different reaction set-up systems: Schlenk line and Parr reactor was investigated and the catalytic results are shown in Table 3.6. For the Schlenk line system (system 1), the reaction was performed in a round-bottom flask equipped with a Schlenk line under nitrogen atmosphere. For the Parr reactor system (system 2), the reaction was performed in a Parr reactor under 10 bar of N_2 pressure. The results show that both systems could completely convert **A** to **B** within 5 h. However, the yield of **B** from system 1 was found to be 28.1 % which was higher than that of system 2 (7.2 %). In terms of the yield of the desired product **C,** system 1 gave 71.9 % yield of **C** which was lower than that obtained from system 2 (92.8 %). This observation might be explained that, upon increasing the N_2 pressure, the catalyst activity for condensation of **B** to **C** was increased substantially [50]. Therefore, based on the above reason, the reaction system performed in a Parr reactor was chosen for further investigation for the catalytic activity of the synthesized trifunctional catalysts.

Table 3.6 Deacetalization-Knoevenagel reaction using two different reaction set-up systems[a]

System	Catalyst	Conversion of A (%)	Yield of B (%)	Yield of C (%)
1[b]	$SA_{0.5}N_4$	100	28.1	71.9
2[c]	$SA_{0.5}N_4$	100	7.2	92.8

[a]Reaction conditions: $SA_{0.5}N_4$ catalyst (0.04 g), **A** (0.15 mmol), malononitrile (1.2 mmol), p-xylene (0.5 mmol, internal standard), temperature 90 ^{o}C and reaction time 5 h

[b]Reaction was performed in a round-bottom flask equipped with Schlenk line under nitrogen atmosphere

[c]Reaction was performed in a Parr reactor under 10 bar of N_2 pressure

3.3 Synthesis of benzylmalononitrile (D)

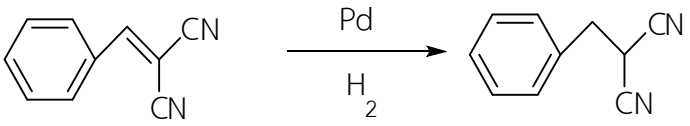

Benzylidenemalononitrile (C) Benzylmalononitrile (D)

Scheme 3.5 Hydrogenation reaction of benzylidene malononitrile (**C**) to produce benzylmalononitrile (**D**).

In order to probe the catalytic activity of the synthesized trifunctional acid-base-metal catalysts, they were used as catalysts in the one-pot deacetalization-Knoevenagel-hydrogenation reaction for the conversion of benzaldehydedimethylacetal (**A**) to benzylmalononitrile (**D**). Due to the lack of a standard sample of **D**, compound **D** was synthesized in the lab and used as the standard for GC measurement. The synthesis of **D** was performed in a Parr reactor by adding benzylidenemalononitrile (**C**), catalyst (5% Pd/Al_2O_3 (commercial)), and toluene in the reactor (Scheme 3.5). After the reaction, the product **D** was purified by column chromatography (hexane:ethyl acetate = 3:1). The product **D** was obtained as a white solid as shown in Fig. 3.18.

Figure 3.18 The appearance of compound **D** after purification.

The identity of compound **D** was confirmed by NMR analysis. The ^{1}H-NMR spectrum of **D** in MeOD (Fig. 3.19) shows two signals for methylene protons (a) at 3.35 ppm as a doublet (2H) and methine proton (b) at 3.41 ppm as a triplet (1H). The signal in the region of 7.21 to 7.32 ppm was a multiplet (5H), corresponding to the phenyl protons.

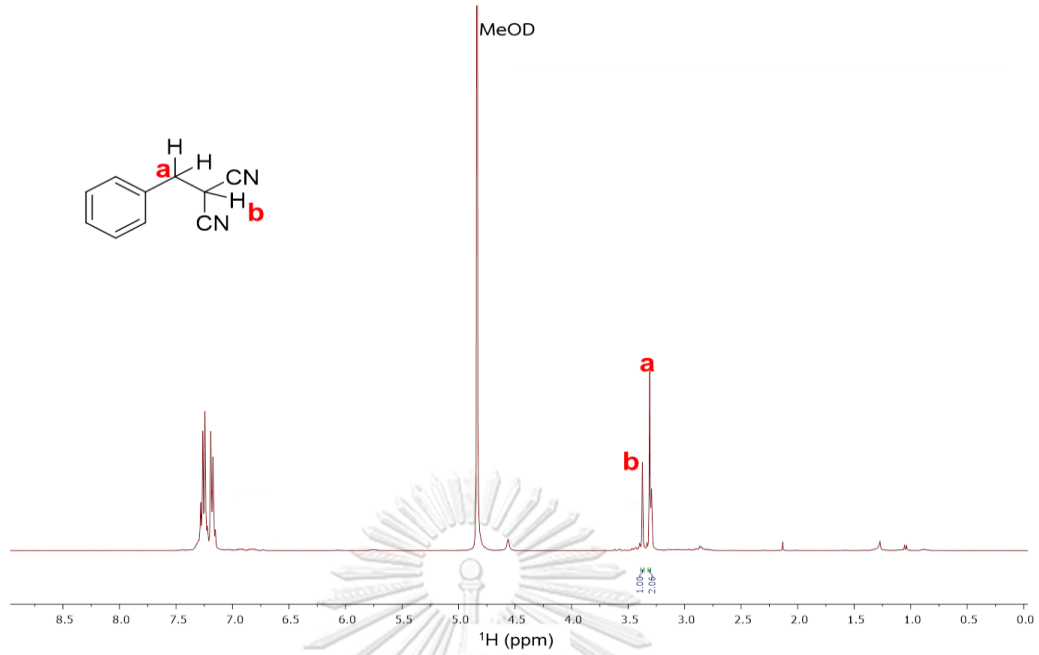

Figure 3.19 ^{1}H-NMR spectrum of **D** after purification (400 MHz, in MeOD).

The ^{13}C-NMR spectrum of **D** in MeOD is shown in Figure 3.20. The signals were at 129.90, 129.71, 128.07, 127.87, 126.02 ppm (aromatic carbon), 121.50 ppm (2CN's), 35.78 (CH_2) and 30.67 (CH). This NMR spectrum is similar to that obtained from a previous report by Jimenez et al [55], confirming the successful synthesis of **D**.

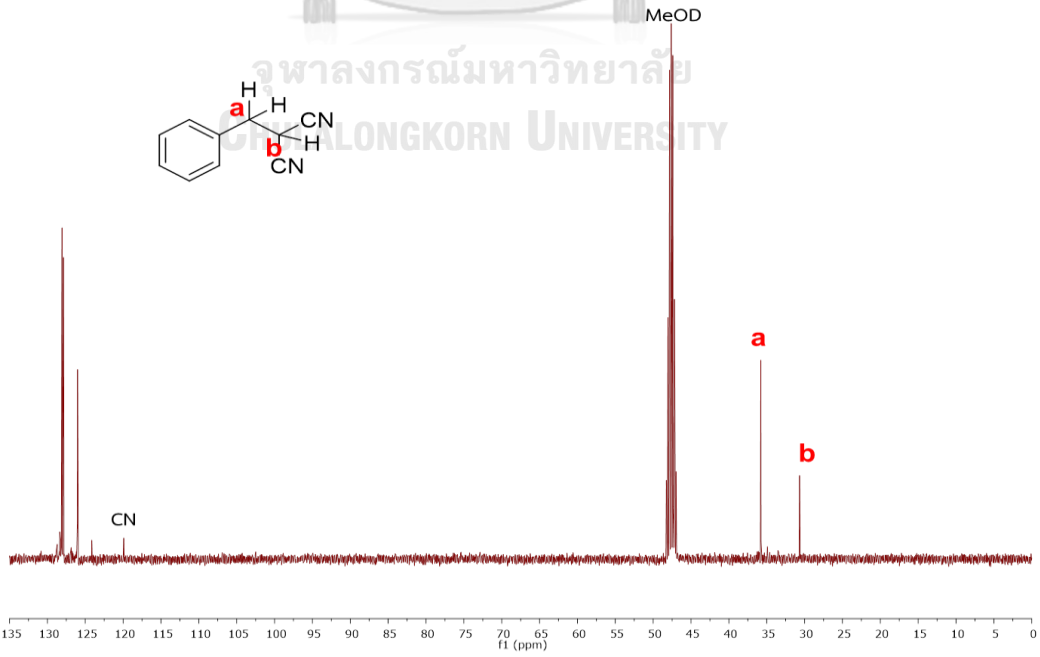

Figure 3.20 ^{13}C-NMR spectrum of **D** after purification (100 MHz, in MeOD).

Moreover, the HSQC (Heteronuclear Single Quantum Coherence) experiment was used to investigate proton-carbon single bond correlations [81], where the protons are along the observed ^{1}H (X) axis and the carbons are along the ^{13}C (Y) axis. The HSQC spectrum of **D** at 400 MHz is shown in Figure 3.21. The spectrum shows the correlations of CH_2 peaks at a position and CH peaks at b position in opposite phase. This observation confirms the results from ^{1}H NMR and ^{13}C NMR described above. The GC chromatogram of **D** was shown in Fig. 3.22.

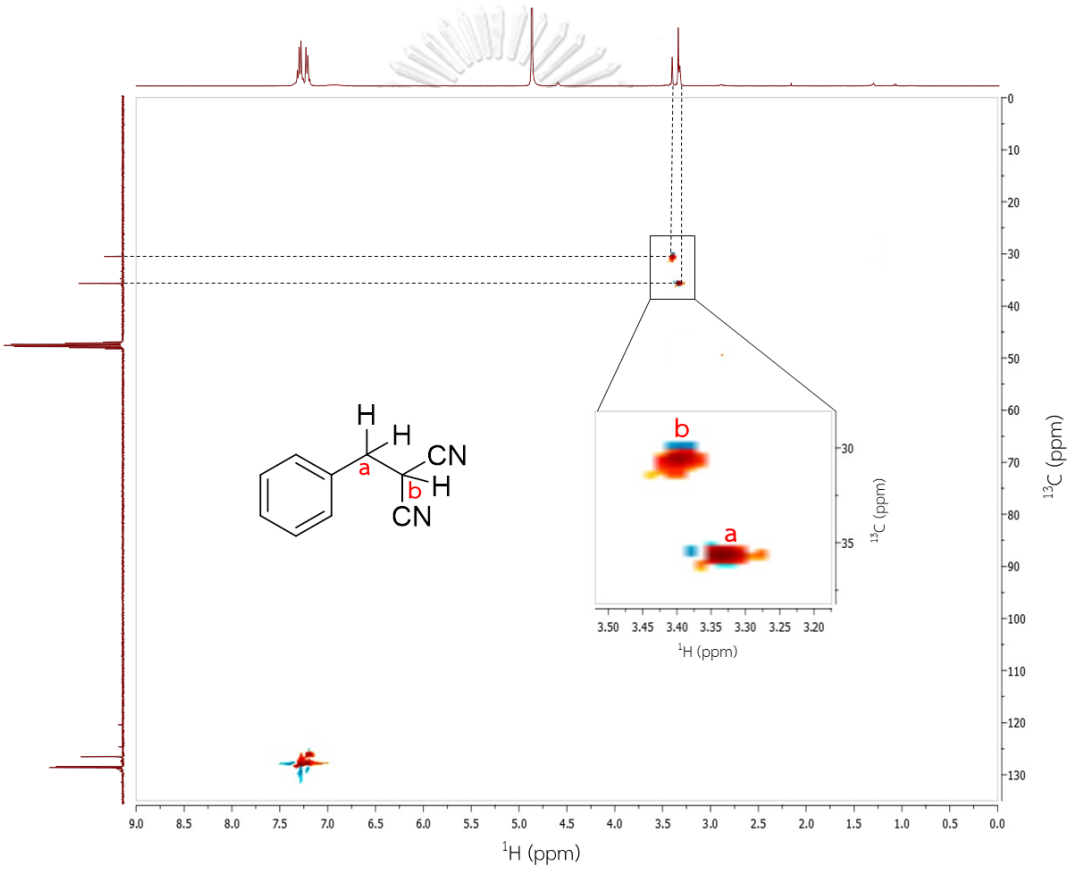

Figure 3.21 HSQC spectrum of **D** after purification in MeOD.

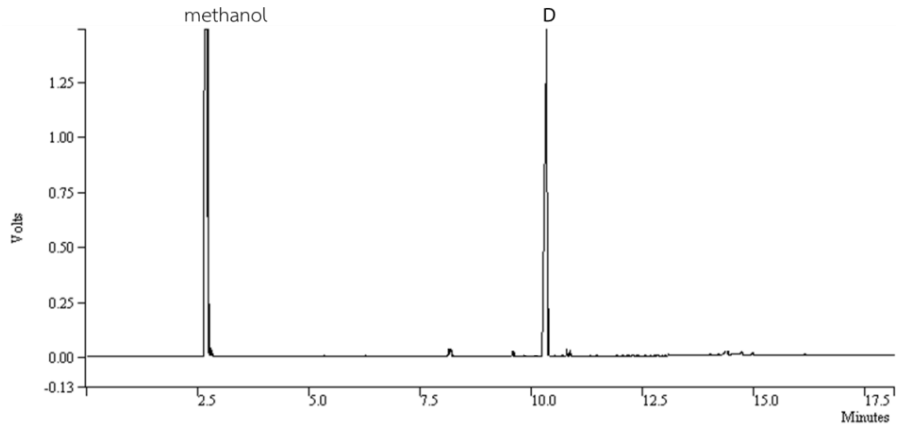

Figure 3.22 GC-FID chromatogram of **D**.

3.4 Catalytic activity of the synthesized trifunctional acid-base-metal catalysts

The synthesized trifunctional acid-base-metal mesoporous catalysts were investigated for their catalytic activities in the one-pot deacetalization-Knoevenagel-hydrogenation reaction. In this work, the catalytic processes were divided into 6 parts:

(I) Effect of Pd loading

(II) Effect of reaction time

(III) Effect of hydrogen pressure

(IV) Effect of types of aminosilanes

(V) Effect of types of gas used in the reaction

The schematic diagram for the one-pot deacetalization-Knoevenagel-hydrogenation reaction was shown in Scheme 3.6. Mechanistically, the acid-catalyzed deacetalization of benzaldehydedimethylacetal (**A**) to produce benzaldehyde (**B**) occurred in the first step, followed by the base-catalyzed Knoevenagel condensation of **B** with malononitrile to produce benzylidenemalononitrile (**C**) in the second step. Finally, metal-catalyzed hydrogenation of benzylidenemalononitrile (**C**) led to the production of benzylmalononitrile (**D**) in the last step.

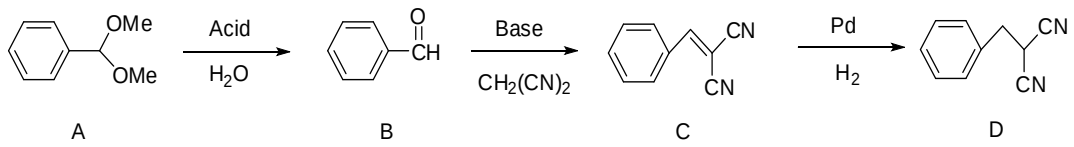

Scheme 3.6 One-pot of deacetylation-Knoevenagel-hydrogenation reaction.

3.4.1 Effect of Pd loading

Three catalysts containing different Pd loadings (0.03, 0.2 and 1 wt.%) with fixed acid (0.5 mmol) and base loadings (4 mmol): $SA_{0.5}N_4Pd_{0.03}$ (entry 1), $SA_{0.5}N_4Pd_{0.2}$ (entry 2) and $SA_{0.5}N_4Pd_1$ (entry 3) were tested to compare their trifunctional activity for the one-pot deacetalization-Knoevenagel-hydrogenation reaction (Table 3.7). The reactions were performed in a Parr reactor under 10 bar of H_2 for 5 h. The results showed that the conversion of **A** using $SA_{0.5}N_4Pd_{0.03}$ was found to be 97.0 % which was higher than using $SA_{0.5}N_4Pd_{0.2}$ (31.5 %), and $SA_{0.5}N_4Pd_1$ (12.2 %). This finding could be described by the acidity of the catalysts. As reported in Table 3.2, the acidity of $SA_{0.5}N_4Pd_{0.03}$ was found to be 0.80 mmol g^{-1} which was higher than that of $SA_{0.5}N_4Pd_{0.2}$ (0.63 mmol g^{-1}) and $SA_{0.5}N_4Pd_1$ (0.38 mmol g^{-1}). Moreover, the yield of **C** using $SA_{0.5}N_4Pd_{0.03}$ was found to be 86.3 % which was higher than using $SA_{0.5}N_4Pd_{0.2}$ (14.6 %) and $SA_{0.5}N_4Pd_1$ (2.7 %), probably because the basicity of $SA_{0.5}N_4Pd_{0.03}$ was found to be 0.44 mmol g^{-1} which was higher than that of $SA_{0.5}N_4Pd_{0.2}$ (0.28 mmol g^{-1}) and $SA_{0.5}N_4Pd_1$ (0.19 mmol g^{-1}). This information suggests that the catalytic activity of the catalysts was decreased with the increase of Pd loading, likely due to the decreasing number of acidic sites and basic sites. However, the desired product **D** was not obtained from these three catalysts, suggesting that the hydrogenation reaction could not occur in the last step.

Table 3.7 Deacetalization–Knoevenagel-hydrogenation reaction catalyzed by trifunctional catalysts[a]

Entry	Materials	Conversion of A (%)	Yield of B (%)	Yield of C (%)	Area percent of D[e] (%)
1	$SA_{0.5}N_4Pd_{0.03}$	97.0	9.2	86.3	N.A.
2	$SA_{0.5}N_4Pd_{0.2}$	31.5	14.1	14.6	N.A.
3	$SA_{0.5}N_4Pd_1$	12.2	4.9	2.1	N.A.
4	$SA_{0.5}N_4Pd_1$[b]	22.5	17.4	2.7	N.A.
5	$SA_{0.5}N_4Pd_1$[c]	15.1	10.4	2.9	N.A.
6	$SA_{0.5}NN_4Pd_{0.2}$	23.3	17.8	5.4	N.A.
7	$SA_{0.5}NNN_4Pd_{0.2}$	19.4	15.1	3.6	N.A.
8	$SA_{0.5}N_4Pd_{0.2}$[d]	100	5.4	59.7	N.A.
9	$SA_{0.5}N_4Pd^{2+}_{0.2}$[d]	91.9	18.2	68.6	N.A.

[a]The reactions were performed in a Parr reactor. Reaction conditions: catalyst (0.04 g), **A** (0.15 mmol), malononitrile (1.2 mmol), p-xylene (0.5 mmol, internal standard), temperature 90 °C, 10 bar of H_2 pressure and 5 h of reaction time.

[b]Reaction time 10 h

[c]Pressure 30 bar

[d]Reaction was performed under nitrogen atmosphere for 5 h, followed by under 10 bar of H_2 for another 5 h.

[e]Area percent of D = (area of D / total area) from GC chromatogram

3.4.2 Effect of reaction time

The one-pot deacetalization-Knoevenagel-hydrogenation reaction using two different reaction times: 5 h and 10 h were investigated using $SA_{0.5}N_4Pd_1$ as

the catalyst (Table 3.7, entries 3-4). When the reaction time was increased from 5 to 10 h, the conversion of **A** was increased from 12.2 % (5 h) to 22.5 % (10 h) while yield of **C** for 10 h of reaction time which was found to be 2.7 % was only slightly higher than the yield of **C** for 5 h of reaction time (2.1 %). The desired product **D** was not observed from both reactions. These results suggest that the increase of reaction time from 5 h to 10 h still did not lead to the production of **D**.

3.4.3 Effect of hydrogen pressure

The one-pot deacetalization-Knoevenagel-hydrogenation reaction using two different pressure of H_2: 10 bar and 30 bar were investigated using $SA_{0.5}N_4Pd_1$ as the catalyst (Table 3.7, entries 3 and 5). The results showed that when the hydrogen pressure was increased from 10 to 30 bar, the conversion of **A** was increased from 12.2 % to 15.1 % while yield of **C** from using hydrogen pressure of 30 bar was found to be 2.9 % which was slightly higher than the yield of **C** from that of 10 bar (2.1 %). The desired product **D** was not observed from both reactions. These results suggest that the increase of hydrogen pressure from 10 bar to 30 bar still did not lead to the production of **D**.

3.4.4 Effect of types of aminosilanes

The effect of types of aminosilanes containing different numbers of amino groups was also studied. Three types of catalysts: $SA_{0.5}N_4Pd_{0.2}$, $SA_{0.5}NN_4Pd_{0.2}$, and $SA_{0.5}NNN_4Pd_{0.2}$ were studied under the hydrogen pressure of 10 bar for 5 h as shown in Table 3.7 (entries 2, 6 and 7). When the number of amino groups was increased from one (N) to three (NNN), the conversion of **A** and yield of **C** were significantly decreased. These results suggest that $SA_{0.5}N_4Pd_{0.2}$ exhibited a higher reactivity than the other two catalysts in terms of conversion of **A** and yield of **C** because it contained the smallest aminosilane molecule, which had least steric hindrance in the reaction to form **C**. This observation was similar to the results from the study of the effect of types of aminosilanes in bifunctional acid-base catalysts in

Section 3.2.4. However, the desired product **D** was not observed from these three reactions.

3.4.5 Effect of types of gas used in the reaction

The one-pot deacetalization-Knoevenagel-hydrogenation reaction using $SA_{0.5}N_4Pd_{0.2}$ as the catalyst was investigated in a Parr reactor at 90 ^{o}C for 5 h under 10 bar of nitrogen atmosphere, followed by 5 h under 10 bar of hydrogen atmosphere (Table 3.7, entry 8). The reason for the use of nitrogen gas, followed by that of hydrogen gas was because the malononitrile substrate could dimerize and trimerize to form the products of dimer (1,1,3-tricyano-2-amino-l-propene) and trimer (1-(aminovinyl)-3-dicyanomethyl-4,5-dicyano-pyrazole), respectively under hydrogen pressure with a Pt-on-alumina catalyst as described by Miki et al [82]. However, in our mechanistic hypothesis, the acid-catalyzed deacetalization of benzaldehydedimethylacetal (**A**) to produce benzaldehyde (**B**) occurred in the first step, followed by the base-catalyzed Knoevenagel condensation of **B** with malononitrile to produce benzylidenemalononitrile (**C**) in the second step. These first two steps were expected to complete or almost complete within 5 h under 10 bar of nitrogen atmosphere. Then, the metal-catalyzed hydrogenation of benzylidenemalononitrile (**C**) to the produce benzylmalononitrile (**D**) in the last step was performed for 5 h under 10 bar of hydrogen atmosphere. The results show that **A** was completely converted within 10 h while the yields of **B** and **C** were found to be 5.4 % and 59.7 %, respectively. In addition, 32.3 % yield of 3-(2-phenylethyl)benzonitrile was also observed from GC-MS measurement. However, the desired product **D** was still not observed from this reaction.

Moreover, the trifunctional acid-base-metal catalyst was prepared to let Pd(II) ions anchor onto the $SA_{0.5}N_4$ material without the reduction process of Pd(II) to Pd(0). The one-pot deacetalization-Knoevenagel-hydrogenation reaction using $SA_{0.5}N_4Pd^{2+}{}_{0.2}$ as the catalyst was investigated in a Parr reactor at 90 ^{o}C for 5 h under 10 bar of nitrogen atmosphere, followed by 5 h under 10 bar of hydrogen atmosphere (Table 3.7, entry 9). The results show that 91.9 % of **A** was converted

within 10 h while the yields of **B** and **C** were found to be 18.2 % and 68.6 %, respectively. However, the desired product **D** was not observed from this catalyst.

It can be seen from the experimental results in Sections 3.4.1-3.4.5 that the reactions did not lead to the formation of the desired product **D**. This might be due to the phenomenon reported by Wang et al. [83]. Specifically, in this study, the trifunctional catalyst was synthesized by the impregnation of aqueous solution of $PdCl_2$ to $SA_{0.5}N_4$. The deactivation of the catalyst might result from the presence of chlorine in $PdCl_2$, which often caused the aggregation of nanoparticles.

3.5 Catalytic testing of one-pot deacetylation-Knoevenagel-hydrogenation reaction using physical mixed catalysts

Due to the unsuccessful use of the synthesized trifunctional catalysts for the one-pot deacetylation-Knoevenagel-hydrogenation reaction, another approach was tested. The new approach was the use of the synthesized bifunctional acid-base catalysts physically mixed with a supported palladium catalyst. Specifically, each of the following three bifunctional acid-base catalysts: $SA_{0.5}N_4$, $SA_{0.5}NN_4$, and $SA_{0.5}NNN_4$ was physically mixed with 5%Pd/Al_2O_3 (commercial) in the weight ratio of 0.4:1. These mixed catalysts were tested for their catalytic activity for the one-pot deacetalization-Knoevenagel-hydrogenation reaction. The reactions were performed in a Parr reactor at 90 ℃ for 5 h under 10 bar of nitrogen atmosphere, followed by 5 h under 10 bar of hydrogen atmosphere. The catalytic activities including conversion of **A**, yield of **B,** yield of **C** and area percent of **D** using the physical mixed catalysts are listed in Table 3.8. The results show that the use of the three catalysts: $SA_{0.5}N_4$ with 5% Pd/Al_2O_3 (entry 1), $SA_{0.5}NN_4$ with 5%Pd/Al_2O_3 (entry 2), and $SA_{0.5}NNN_4$ with 5% Pd/Al_2O_3 (entry 3) gave similar conversion of **A** (52.2-59.4%). This finding can be explained by the similar acidity of the catalysts (~0.9 mmol g^{-1}). Interestingly, the product **D** was observed from all of the three reactions by the effect of Pd/Al_2O_3. Specifically, area percent of **D** using $SA_{0.5}N_4$ + 5%Pd/Al_2O_3 was found to be 49.4 % which was higher than that of $SA_{0.5}NN_4$ + 5%Pd/Al_2O_3 (18.2 %), and $SA_{0.5}NNN_4$ + 5%Pd/Al_2O_3 (11.3 %), respectively. This observation was similar to the results from

Section 3.2.4: Effect of aminosilane types in bifunctional catalysts described earlier. Specifically, $SA_{0.5}N_4$ exhibited a higher activity than the other two catalysts ($SA_{0.5}NN_4$ and $SA_{0.5}NNN_4$) and therefore gave the highest yield of **C**. Consequently, the metal-catalyzed hydrogenation of benzylidenemalononitrile (**C**) using $SA_{0.5}N_4$ + 5%Pd/Al_2O_3 as the catalyst led to the highest yield of benzylmalononitrile (**D**) in the last step.

Moreover, the bifunctional acid-base $SA_{0.5}N_4$ catalyst was also physically mixed with a less amount of 5%Pd/Al_2O_3 (commercial) in the weight ratio of 1:0.2 so that the Pd concentration was the same as the one in the trifunctional $SA_{0.5}N_4Pd_1$catalyst (Table 3.8, entry 4). The results show that the area percent of **D** was found to be 5.2%.

Table 3.8 Deacetalization-Knoevenagel-hydrogenation reaction catalyzed by using physical mixed catalysts

Entry	Materials	Conversion of **A** (%)	Yield of **B** (%)	Yield of **C** (%)	Area percent of **D** (%)
1	$SA_{0.5}N_4$ +5% Pd/Al_2O_3	59.4	1.7	6.6	49.4
2	$SA_{0.5}NN_4$ +5% Pd/Al_2O_3	52.2	23.6	10.2	18.2
3	$SA_{0.5}NNN_4$ +5% Pd/Al_2O_3	58.4	37.4	8.6	11.3
4	$SA_{0.5}N_4$ +5% Pd/Al_2O_3[b]	67.2	8.2	49.9	5.2

[a]The reactions were performed in a Parr reactor. Reaction conditions: physical mixed catalysts: 40 mg of $SA_{0.5}N_4$, $SA_{0.5}NN_4$, or $SA_{0.5}NNN_4$ and 100 mg of 5% Pd/Al_2O_3 (commercial), **A** (0.15 mmol), malononitrile (1.2 mmol), p-xylene (0.5 mmol, internal standard), temperature 90 $^{\circ}C$, 10 bar of nitrogen atmosphere for 5 h, followed by under 10 bar of H_2 for another 5 h.

[b]Physical mixed catalysts: 40 mg of $SA_{0.5}N_4$ and 8 mg of 5% Pd/Al_2O_3 (commercial).

CHAPTER IV
CONCLUSIONS

The bifunctional mesoporous silica-supported acid (-SO_3H)-base (-NH_2) catalysts were synthesized using a combination of co-condensation and post-synthetic grafting methods. Eight bifunctional catalysts with different site-separation, acid loading, base loading, and type of aminoosilane were prepared including N_2SA_2, $SA_{0.5}N_{0.5}$, $SA_{0.5}N_2$, SA_1N_2, SA_2N_2, $SA_{0.5}N_4$, $SA_{0.5}NN_4$ and $SA_{0.5}NNN_4$ catalysts.

The synthesized acid-base catalysts were characterized by XRD, FT-IR, N_2 adsorption-desorption, SEM, TEM, TGA and XPS techniques. The TEM results agreed well with the XRD results for the formation of ordered mesoporous structure. The results from N_2 adsorption-desorption indicated that the surface area of the catalysts were in the range of 609-729 m^2 g^{-1}. The S=O and N-H stretching frequencies, as indicated by FT-IR, occurred at 1,032 and 1,536 cm^{-1}, respectively. The acid and base concentrations of the catalysts, examined by back titration method, were in the range of 0.88-1.10 mmol g^{-1} and 0.29-0.57 mmol g^{-1}, respectively. The SEM results indicate that their structures were small kidney-bean-shaped rods. The bifunctional materials could be performed at temperature below 200 °C without degradation from TGA. The XPS result confirms that most of the –SH groups were converted to the sulfonic acid groups (-SO_3H) by using H_2O_2 and acetic acid.

The synthesized bifunctional catalysts were tested for the one-pot deacetylation-Knoevenagel reaction of benzaldehydedimethylacetal (**A**) with malononitrile to produce benzylidenemalononitrile (**C**) at 90 $^{\circ}C$ for 5 h. The results show that the conversion of **A** and the yield of **C** were influenced by pore characteristics, acidity and basicity of the catalysts. In particular, $SA_{0.5}N_4$ exhibited the highest conversion of **A** (100%) and the highest yield of **C** (71%). Moreover, the substitution of malononitrile with ethyl cyanoacetate was successful in the one-pot deacetalization-Knoevenagel reaction, which gave 63% yield of ethyl trans-**α**-

cyanocinnamate (**C_2**). For the reusability test, the $SA_{0.5}N_4$ catalyst showed a good maintenance of activity at least four times without a significant decrease in activity.

Then, trifunctional acid-base-metal catalysts were prepared by impregnation of palladium metal (0.03, 0.2 and 1 wt%) on the $SA_{0.5}N_4$ bifunctional acid-base material. Three modified materials including $SA_{0.5}N_4Pd_{0.03}$, $SA_{0.5}N_4Pd_2$ and $SA_{0.5}N_4Pd_1$ were obtained. These catalysts were tested for one-pot deacetylation-Knoevenagel-hydrogenation reaction (**A** to **D**). The effects of reaction time, hydrogen pressure, Pd loading and types of aminosilanes were investigated. Unfortunately, the desired product benzylmalononitrile (**D**) was not observed in any conditions employed.

Moreover, the one-pot deacetylation-Knoevenagel-hydrogenation reaction was also tested using the physical mixed catalysts: $SA_{0.5}N_4$, $SA_{0.5}NN_4$, or $SA_{0.5}NNN_4$ and 5%Pd/Al_2O_3 (commercial). The results show that the production of **D** was observed. Specifically, the area percent of **D** using $SA_{0.5}N_4$+5%Pd/Al_2O_3 was found to be 49.4 % which was higher than that of $SA_{0.5}NN_4$+5%Pd/Al_2O_3 (18.2 %), and $SA_{0.5}NNN_4$+5% Pd/Al_2O_3 (11.3 %), respectively.

Suggestion for future work: internal surface of MCM-41 is functinalized with aminosilanes groups, followed by partial protonation of amino groups using tungstophosphoric acid. In the last step, Pd nanoparticles are impregnated on some amino groups.

REFERENCES

[1] Explainer: What is a catalyst? [Online]. Available from: https://www.sciencenewsforstudents.org/article/explainer-catalyst-chemistry [2018, May 7]

[2] How does a catalyst actually lower the activation energy of a reaction? [Online]. Available from: https://www.quora.com/How-does-a-catalyst-actually-lower-the-activation-energy-of-a-reaction [2018, May 7]

[3] Reaction Rates [Online]. Available from: http://slideplayer.com/slide/10788240/ [2018, May 9]

[4] THE EFFECT OF CATALYSTS ON REACTION RATES [Online]. Available from: https://www.chemguide.co.uk/physical/basicrates/catalyst.html [2018, May 9]

[5] Catalysts (SL) [Online]. Available from: https://www.youtube.com/watch?v=nw8bg7vkezY [2018, May 9]

[6] TYPES OF CATALYSIS [Online]. Available from: https://www.chemguide.co.uk/physical/catalysis/introduction.html [2018, May 7]

[7] Homogeneous catalysis [Online]. Available from: http://nptel.ac.in/courses/103103026/pdf/mod3.pdf [2018, May 8]

[8] Catalysis [Online]. Available from: https://courses.lumenlearning.com/boundless-chemistry/chapter/catalysis/ [2018, May 8]

[9] Mishra, S., Balyan, S., Pant, K.K., and Haider, M.A. Non-oxidative conversion of methane into higher hydrocarbons over Mo/MCM-22 catalyst. Journal of Chemical Sciences (2017).

[10] Yusoff, M.H.M. and Abdullah, A.Z. Catalytic behavior of sulfated zirconia supported on SBA-15 as catalyst in selective glycerol esterification with palmitic acid to monopalmitin. Journal of the Taiwan Institute of Chemical Engineers 60 (2016): 199-204.

[11] Le Page, I.F. Applied heterogenous catalysis : design manufacture use of solid catalysis. Paris :: Technip, 1987.

[12] Guldhe, A., Singh, P., Ansari, F.A., Singh, B., and Bux, F. Biodiesel synthesis from microalgal lipids using tungstated zirconia as a heterogeneous acid catalyst and its comparison with homogeneous acid and enzyme catalysts. Fuel 187(Supplement C) (2017): 180-188.

[13] Ispir, E., Sahin, E., Ikiz, M., and Aktas, A. Comparative transfer hydrogenation performance of homogeneous and heterogeneous ruthenium (II) catalysts derived from a Schiff base ligand. Journal of Organometallic Chemistry 830(Supplement C) (2017): 188-195.

[14] Catalysis [Online]. Available from: https://courses.lumenlearning.com/boundless-chemistry/chapter/catalysis/ [2018, May 11]

[15] Homogeneous vs. heterogeneous catalysis [Online]. Available from: https://www.catalysis.de/fileadmin/user_upload/MAIN-dateien/1Forschung/FB_Rosenthal/Probevorlesung_Hapke_Hand-out.pdf [2018, May 8]

[16] Major differences between homogeneous and heterogeneous catalysts [Online]. Available from: http://webcache.googleusercontent.com/search?q=cache:fMsx2_s68WsJ:web.uvic.ca/~mcindoe/423/homovshet.pdf+&cd=8&hl=th&ct=clnk&gl=th [2018, May 8]

[17] Akhtar, F., Andersson, L., Ogunwumi, S., Hedin, N., and Bergström, L. Structuring adsorbents and catalysts by processing of porous powders. Journal of the European Ceramic Society 34(7) (2014): 1643-1666.

[18] Zdravkov, B.D., Čermák, J.J., Šefara, M., and Janků, J. Pore classification in the characterization of porous materials: A perspective. Central European Journal of Chemistry 5(2) (2007): 385-395.

[19] Chudasama, C.D., Sebastian, J., and Jasra, R.V. Pore-Size Engineering of Zeolite A for the Size/Shape Selective Molecular Separation. Industrial & Engineering Chemistry Research 44(6) (2005): 1780-1786.

[20] Barton, T.J., et al. Tailored Porous Materials. Chemistry of Materials 11(10) (1999): 2633-2656.

[21] Surfactant [Online]. Available from: https://en.wikipedia.org/wiki/Surfactant [2018, May 16]

[22] What Are Surfactants [Online]. Available from: http://www.bristol.ac.uk/chemistry/research/eastoe/what-are-surfactants/ [2018, May 16]

[23] Alothman, Z. A Review: Fundamental Aspects of Silicate Mesoporous Materials. Materials 5(12) (2012): 2874-2902.

[24] Samiey, B., Cheng, C.H., and Wu, J. Organic-Inorganic Hybrid Polymers as Adsorbents for Removal of Heavy Metal Ions from Solutions: A Review. Materials (Basel) 7(2) (2014): 673-726.

[25] Samiey, B., Cheng, C.-H., and Wu, J. Organic-Inorganic Hybrid Polymers as Adsorbents for Removal of Heavy Metal Ions from Solutions: A Review. Materials 7(2) (2014): 673-726.

[26] Beck, J.S., et al. A new family of mesoporous molecular sieves prepared with liquid crystal templates. Journal of the American Chemical Society 114(27) (1992): 10834-10843.

[27] Inagaki, S., Fukushima, Y., and Kuroda, K. Synthesis of highly ordered mesoporous materials from a layered polysilicate. Journal of the Chemical Society, Chemical Communications (8) (1993): 680-682.

[28] Ahmad, M. Pores Functionalized Mesoporous Silica: An Original Approach for Hybrid Catalytic Materials. Current Organic Chemistry 18(18) (2014): 2451-2460.

[29] Hoffmann, F., Cornelius, M., Morell, J., and Froba, M. Silica-based mesoporous organic-inorganic hybrid materials. Angew Chem Int Ed Engl 45(20) (2006): 3216-51.

[30] Parida, K., Rath, D., and Rana, S. ChemInform Abstract: Organic Amine-Functionalized Silica-Based Mesoporous Materials: An Update of Syntheses and Catalytic Applications. Vol. 46, 2014.

[31] Huang, Y., Trewyn, B.G., Chen, H.-T., and Lin, V.S.Y. One-pot reaction cascades catalyzed by base- and acid-functionalized mesoporous silica nanoparticles. New Journal of Chemistry 32(8) (2008): 1311-1313.

[32] Szajna-Fuller, E., et al. Kinetics of oxidation of an organic amine with a Cr(V) salen complex in homogeneous aqueous solution and on the surface of mesoporous silica. Dalton Transactions (17) (2009): 3237-3246.

[33] Rapp, J.L., Huang, Y., Natella, M., Cai, Y., Lin, V.S.Y., and Pruski, M. A solid-state NMR investigation of the structure of mesoporous silica nanoparticle supported rhodium catalysts. Solid State Nuclear Magnetic Resonance 35(2) (2009): 82-86.

[34] Suzuki, T.M., Nakamura, T., Fukumoto, K., Yamamoto, M., Akimoto, Y., and Yano, K. Direct synthesis of amino-functionalized monodispersed mesoporous silica spheres and their catalytic activity for nitroaldol condensation. Journal of Molecular Catalysis A: Chemical 280(1) (2008): 224-232.

[35] Anastas, P.T. Introduction: Green Chemistry. Chemical Reviews 107(6) (2007): 2167-2168.

[36] Cooper, G.M. The Cell: A Molecular Approach. 2nd edition ed., 2000.

[37] Townsend, C.A. Structural studies of natural product biosynthetic proteins. Chemistry & Biology 4(10) (1997): 721-730.

[38] Chng, L.L., Erathodiyil, N., and Ying, J.Y. Nanostructured Catalysts for Organic Transformations. Accounts of Chemical Research 46(8) (2013): 1825-1837.

[39] Alauzun, J., Mehdi, A., Reyé, C., and Corriu, R.J.P. Mesoporous Materials with an Acidic Framework and Basic Pores. A Successful Cohabitation. Journal of the American Chemical Society 128(27) (2006): 8718-8719.

[40] Gelman, F., Blum, J., and Avnir, D. One-Pot Reactions with Opposing Reagents: Sol–Gel Entrapped Catalyst and Base. Journal of the American Chemical Society 122(48) (2000): 11999-12000.

[41] Motokura, K., Fujita, N., Mori, K., Mizugaki, T., Ebitani, K., and Kaneda, K. An Acidic Layered Clay Is Combined with A Basic Layered Clay for One-Pot

Sequential Reactions. Journal of the American Chemical Society 127(27) (2005): 9674-9675.

[42] Akagawa, K., Sakamoto, S., and Kudo, K. Resin-supported acid- and base-catalyzed one-pot sequential reaction including an enantioselective step. Tetrahedron Letters 48(6) (2007): 985-987.

[43] Abu-Reziq, R., Wang, D., Post, M., and Alper, H. Separable Catalysts in One-Pot Syntheses for Greener Chemistry. Chemistry of Materials 20(7) (2008): 2544-2550.

[44] Zhang, W., et al. Phosphotungstic Acid Immobilized on Amine-Grafted Graphene Oxide as Acid/Base Bifunctional Catalyst for One-Pot Tandem Reaction. Industrial & Engineering Chemistry Research 53(4) (2014): 1437-1441.

[45] Elmekawy, A.A., Shiju, N.R., Rothenberg, G., and Brown, D.R. Environmentally Benign Bifunctional Solid Acid and Base Catalysts. Industrial & Engineering Chemistry Research 53(49) (2014): 18722-18728.

[46] Iosif, F., et al. Ir-Beta zeolite as a heterogeneous catalyst for the one-pot transformation of citronellal to menthol. Chemical Communications (11) (2004): 1292-1293.

[47] Li, P., Yu, Y., Liu, H., Cao, C.-Y., and Song, W.-G. A core-shell-satellite structured Fe3O4@MS-NH2@Pd nanocomposite: a magnetically recyclable multifunctional catalyst for one-pot multistep cascade reaction sequences. Nanoscale 6(1) (2014): 442-448.

[48] Phan, N.T., Gill, C.S., Nguyen, J.V., Zhang, Z.J., and Jones, C.W. Expanding the utility of one-pot multistep reaction networks through compartmentation and recovery of the catalyst. Angew Chem Int Ed Engl 45(14) (2006): 2209-12.

[49] Chen, Y.Z., Hwang, C.M., and Liaw, C.W. One-step synthesis of methyl isobutyl ketone from acetone with calcined Mg/Al hydrotalcite-supported palladium or nickel catalysts. Applied Catalysis A: General 169(2) (1998): 207-214.

[50] Biradar, A.V., Patil, V.S., Chandra, P., Doke, D.S., and Asefa, T. A trifunctional mesoporous silica-based, highly active catalyst for one-pot, three-step cascade reactions. Chemical Communications 51(40) (2015): 8496-8499.

[51] Krylov, I.B. and Terent'ev, A.O. Oxidative C-O coupling of benzylmalononitrile with 3-(hydroxyimino)pentane-2,4-dione. Russian Journal of Organic Chemistry 51(1) (2015): 10-13.

[52] Sammelson, R., Tayyari, F., Wood, D., and Fanwick, P. Monosubstituted Malononitriles: Efficient One-Pot Reductive Alkylations of Malononitrile with Aromatic Aldehydes. Synthesis 2008(2) (2008): 279-285.

[53] Zhang, Z., Gao, J., Xia, J.-J., and Wang, G.-W. Solvent-free mechanochemical and one-pot reductive benzylizations of malononitrile and 4-methylaniline using Hantzsch 1,4-dihydropyridine as the reductant. Organic & Biomolecular Chemistry 3(9) (2005): 1617-1619.

[54] Wu, J. and Jiang, H. Rh-Catalyzed One-Pot Reductive Alkylation of Malononitrile Under Transfer Hydrogenation Conditions. Synthetic Communications 41(8) (2011): 1218-1226.

[55] Jimenez, D.E.Q., Ferreira, I.M., Birolli, W.G., Fonseca, L.P., and Porto, A.L.M. Synthesis and biocatalytic ene-reduction of Knoevenagel condensation compounds by the marine-derived fungus Penicillium citrinum CBMAI 1186. Tetrahedron 72(46) (2016): 7317-7322.

[56] Varadwaj, G.B.B., Rana, S., Parida, K., and Nayak, B.B. Journal of Materials Chemistry A 2(20) (2014): 7526.

[57] Huang, Y., Xu, S., and Lin, V.S.Y. Angewandte Chemie International Edition 50(3) (2011): 661-664.

[58] Li, P., Cao, C.Y., Chen, Z., Liu, H., Yu, Y., and Song, W.G. Core-shell structured mesoporous silica as acid-base bifunctional catalyst with designated diffusion path for cascade reaction sequences. Chem Commun (Camb) 48(85) (2012): 10541-3.

[59] Quantitation Methods in Gas Chromatography [Online]. Available from: researchgate.net/file.PostFileLoader.html%3Fid%3D555c36f95f7f71ae908b45b3%26assetKey%3DAS:273780985794561%401442285881873+&cd=1&hl=th&ct=clnk&gl=th [2018, May 8]

[60] Huh, S., Wiench, J.W., Yoo, J.-C., Pruski, M., and Lin, V.S.Y. Organic Functionalization and Morphology Control of Mesoporous Silicas via a Co-

Condensation Synthesis Method. Chemistry of Materials 15(22) (2003): 4247-4256.

[61] Mukhopadhyay, K., Sarkar, B.R., and Chaudhari, R.V. Anchored Pd Complex in MCM-41 and MCM-48: Novel Heterogeneous Catalysts for Hydrocarboxylation of Aryl Olefins and Alcohols. Journal of the American Chemical Society 124(33) (2002): 9692-9693.

[62] Shang, F., Sun, J., Wu, S., Yang, Y., Kan, Q., and Guan, J. Microporous and Mesoporous Materials 134(1) (2010): 44-50.

[63] Shang, F., Sun, J., Liu, H., Wang, C., Guan, J., and Kan, Q. One-pot cascade reactions catalyzed by acid–base mesoporous MCM-41 materials. Materials Research Bulletin 47(3) (2012): 801-806.

[64] Chen, Y., Cao, Y., Suo, Y., Zheng, G.-P., Guan, X.-X., and Zheng, X.-C. Mesoporous solid acid catalysts of 12-tungstosilicic acid anchored to SBA-15: Characterization and catalytic properties for esterification of oleic acid with methanol. Journal of the Taiwan Institute of Chemical Engineers 51 (2015): 186-192.

[65] Kamalakar, G., Komura, K., and Sugi, Y. Tungstophosphoric acid supported on MCM-41 mesoporous silicate: An efficient catalyst for the di-tert-butylation of cresols with tert-butanol in supercritical carbon dioxide. Applied Catalysis A: General 310 (2006): 155-163.

[66] Nishi, Y. and Inagaki, M. Chapter 11 - Gas Adsorption/Desorption Isotherm for Pore Structure Characterization. in Materials Science and Engineering of Carbon, pp. 227-247: Butterworth-Heinemann, 2016.

[67] Huang, Y., Xu, S., and Lin, V.S.Y. Bifunctionalized Mesoporous Materials with Site-Separated Brønsted Acids and Bases: Catalyst for a Two-Step Reaction Sequence. Angewandte Chemie International Edition 50(3) (2011): 661-664.

[68] Geng, T., Li, Q., Jiang, Y., and Wang, W. Esterification of Stearic Acid with Triethanolamine over Zirconium Sulfate Supported on SBA-15 Mesoporous Molecular Sieve. Journal of Surfactants and Detergents 14(1) (2011): 15-22.

[69] Yadav, G.D. and Murkute, A.D. Advanced Synthesis & Catalysis 346(4) (2004): 389-394.

[70] Zhang, F., Jiang, H., Li, X., Wu, X., and Li, H. ACS Catalysis 4(2) (2013): 394-401.

[71] Rostamnia, S., Rahmani, T., and Xin, H. Pd(PrSO3)2@SBA-15 and Pd-NPs(PrSO3)@SBA-15 hybrid materials: A highly active, reusable, and selective interface catalyst for C–X activations in air and water. Journal of Industrial and Engineering Chemistry 32 (2015): 218-224.

[72] Biradar, A., Patil, V., Chandra, P., Doke, D., and Asefa, T. Trifunctional Mesoporous Silica-Based, Highly Active Catalyst for One-Pot, Three-Step Cascade Reactions. Vol. 51, 2015.

[73] Shylesh, S., Wagner, A., Seifert, A., Ernst, S., and Thiel, W.R. Chemistry – A European Journal 15(29) (2009): 7052-7062.

[74] Rana, S., Maddila, S., Pagadala, R., and Jonnalagadda, S.B. Synthesis and characterization of novel bifunctional mesoporous silica catalyst and its scope for one-pot deacetalization–knoevenagel reaction. Journal of Porous Materials 22(2) (2015): 353-360.

[75] Li, P., Cao, C.-Y., Chen, Z., Liu, H., Yu, Y., and Song, W.-G. Core-shell structured mesoporous silica as acid-base bifunctional catalyst with designated diffusion path for cascade reaction sequences. Chemical Communications 48(85) (2012): 10541-10543.

[76] Yang, Y., et al. A yolk-shell nanoreactor with a basic core and an acidic shell for cascade reactions. Angew Chem Int Ed Engl 51(36) (2012): 9164-8.

[77] Mu, M., Yan, X., Li, Y., and Chen, L. Post-modified acid-base bifunctional MIL-101(Cr) for one-pot deacetalization-Knoevenagel reaction. Journal of Nanoparticle Research 19(4) (2017): 148.

[78] Suzuki, T.M., Nakamura, T., Fukumoto, K., Yamamoto, M., Akimoto, Y., and Yano, K. Journal of Molecular Catalysis A: Chemical 280(1) (2008): 224-232.

[79] pH and pKa Relationship: The Henderson-Hasselbalch Equation [Online]. Available from: https://www.thoughtco.com/the-ph-and-pka-relationship-603643 [2018, May 7]

[80] Valvekens, P., Vandichel, M., Waroquier, M., Van Speybroeck, V., and De Vos, D. Metal-dioxidoterephthalate MOFs of the MOF-74 type: Microporous basic catalysts with well-defined active sites. Journal of Catalysis 317 (2014): 1-10.

[81] Cavanagh, J., Fairbrother, W.J., Palmer Iii, A.G., Rance, M., and Skelton, N.J. CHAPTER 7 - HETERONUCLEAR NMR EXPERIMENTS. in Protein NMR Spectroscopy (Second Edition), pp. 533-678. Burlington: Academic Press, 2007.

[82] Miki, M., Yanagimachi, H., Kashiki, I., Sakai, M., and Suzuki, A. Kinetics of Polymerization of Malononitrile under Hydrogen Pressure. 2018.

[83] Wang, Y., Deng, Y., and Shi, F. Active palladium catalyst preparation for hydrogenation reactions of nitrobenzene, olefin and aldehyde derivatives. Journal of Molecular Catalysis A: Chemical 395 (2014): 195-201.

APPENDIX

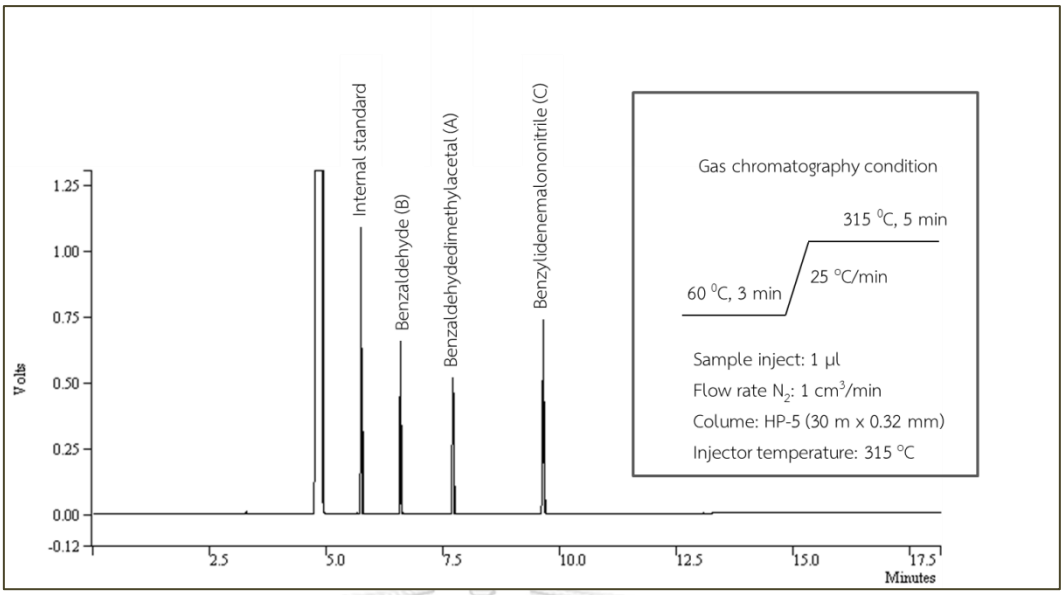

Figure A-1 Gas chromatogram showing the sample analysis of benzylidenemalononitrile (**C**) products from one-pot deacetylation-Knoevenagel reaction of benzaldehydedimethylacetal (**A**) with malononitrile using p-xylene as the internal standard.

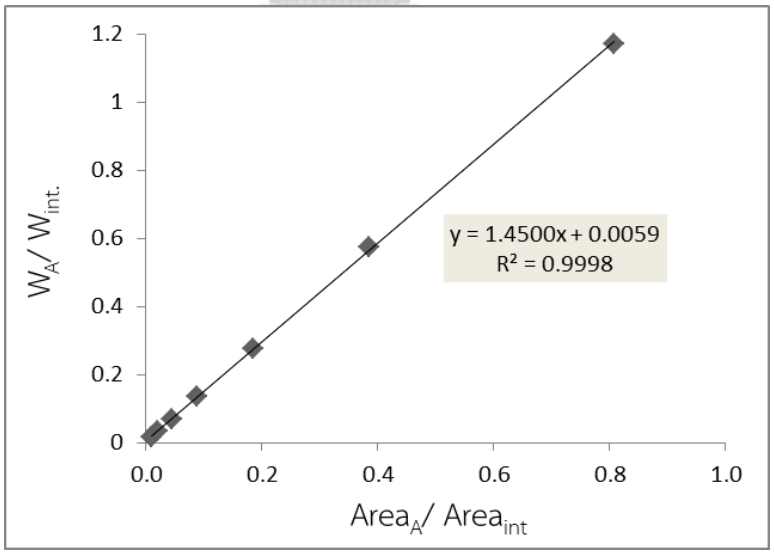

Figure A-2 Calibration curve of benzaldehydedimethylacetal (**A**) analyzed by GC using p-xylene as the internal standard.

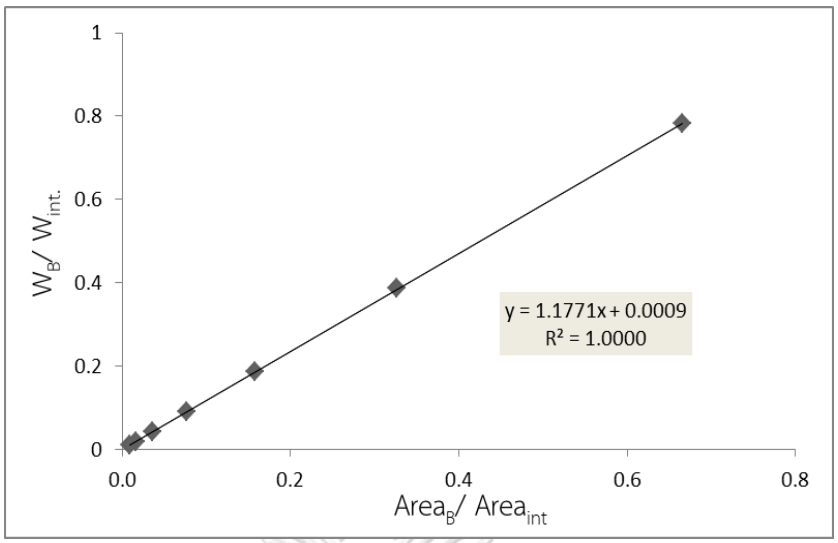

Figure A-3 Calibration curve of benzaldehyde (**B**) analyzed by GC using p-xylene as the internal standard.

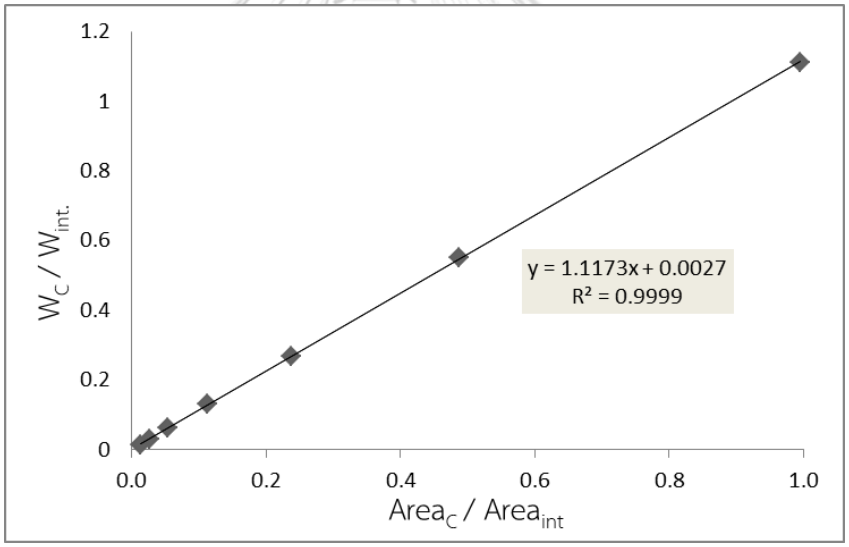

Figure A-4 Calibration curve of benzalidenemalononitrile (**C**) analyzed by GC using p-xylene as the internal standard.

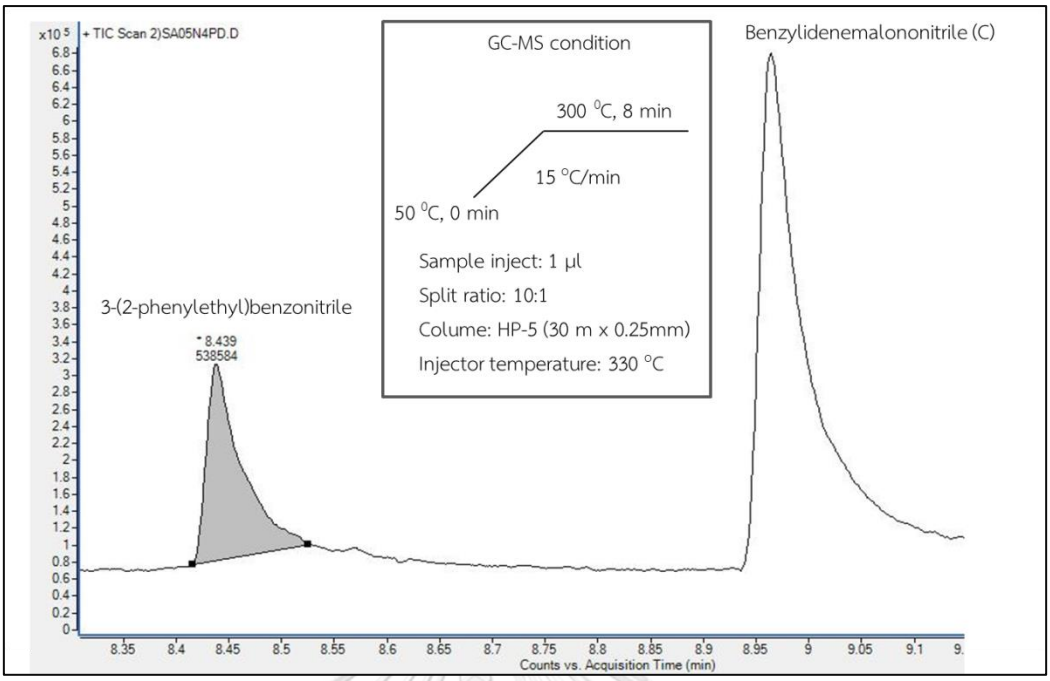

Figure A-5 Gas chromatogram showing the sample analysis of 3-(2-phenylethyl)benzonitrile byproduct from one-pot deacetylation-Knoevenagel-hydrogenation reaction of benzaldehydedimethylacetal (**A**) with malononitrile.

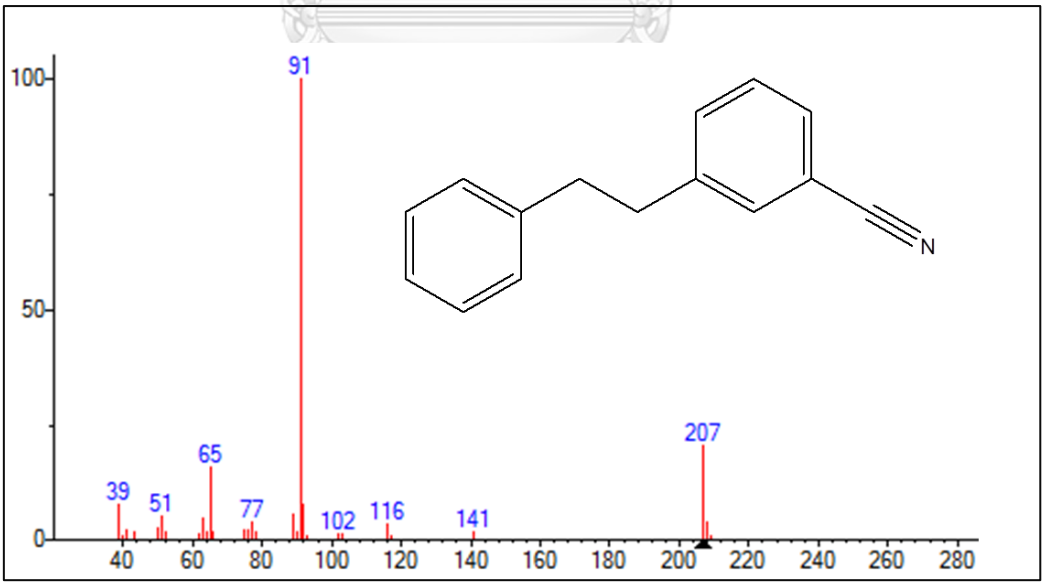

Figure A-6 Mass spectrum of 3-(2-phenylethyl)benzonitrile.

VITA

Mr. Apichat Klayanon was born on October 17, 1993 in Angthong, Thailand. He graduated with Bachelor's Degree in Chemistry from Faculty of Science, Burapha University in 2015. In addition, he continued his study in Inorganic chemistry, Faculty of Science, Chulalongkorn University in 2015 and he has completed his study in a Master's Degree in Chemistry in 2018. He presented his research in Pure and Applied Chemistry International Conference (PACCON 2018) in the topic of "Synthesis of mesoporous silica with site-isolated acid and base – based catalysts and their bifunctional application in a one-pot cascade reaction". His present address is 21/4, Moo 10, Banit, Muang, Angthong, Thailand 14000. E-mail address: apichat24289@hotmail.com Mobile: 086-3064613